This article has been accepted for publication in IEEE Transactions on Wireless Communications. This is the author's version which has not been fully edited and content may change prior to final publication. Citation information: DOI 10.1109/TWC.2025.3633615

MIMO-OFDM Signaling Design for Noncoherent Distributed ISAC Systems

Kawon Han, *Member, IEEE,* Kaitao Meng, *Member, IEEE,* and Christos Masouros, *Fellow, IEEE*

***Abstract*—The ultimate goal of enabling sensing through the cellular network is to obtain coordinated sensing of an unprecedented scale, through distributed integrated sensing and communication (D-ISAC). This, however, introduces challenges related to synchronization and demands new transmission methodologies. In this paper, we propose a transmit signal design framework for noncoherent D-ISAC systems, where multiple ISAC nodes cooperatively perform sensing and communication without requiring phase-level synchronization. The proposed framework employing orthogonal frequency division multiplexing (OFDM) jointly designs downlink coordinated multi-point (CoMP) communication and multi-input multi-output (MIMO) radar waveforms. This leverages both collocated and distributed MIMO radars to estimate angle-of-arrival (AOA) and time-of-flight (TOF) from all possible multi-static measurements for target localization. To this end, we use the target localization Cramér-Rao bound (CRB) as the sensing performance metric and the signal-to-interference-plus-noise ratio (SINR) as the communication performance metric. Then, an optimization problem is formulated to minimize the localization CRB while maintaining a minimum SINR requirement for each communication user. Particularly, we present three distinct transmit signal design approaches, including unconstrained, orthogonal, and beamforming designs, which reveal trade-offs between ISAC performance and computational complexity. Unlike single-node ISAC systems, the proposed D-ISAC designs involve per-subcarrier sensing signal optimization to enable accurate TOF estimation, which contributes to the target localization performance. Numerical simulations demonstrate the effectiveness of the proposed designs in achieving flexible ISAC trade-offs and efficient D-ISAC signal transmission.**

***Index Terms*—Coordinated multipoint (CoMP), Cramér-Rao bound (CRB), distributed integrated sensing and communication (D-ISAC), multi-input multi-output (MIMO) radar.**

I. INTRODUCTION

With the exponential growth in demand for the efficient use of wireless resources, integrated sensing and communication (ISAC) technologies have emerged as an innovative technology, garnering significant attention across academic and industrial sectors [2]–[4]. ISAC systems unify radar sensing and communication functionalities, leveraging common hardware and resources to achieve dual-purpose operations. This integrated approach not only optimizes spectral utilization but also substantially reduces hardware costs and energy consumption, making it a highly efficient alternative to the traditional independent deployment of communication and radar systems [5], [6].

A preliminary version of this paper was presented at 2025 IEEE International Radar Conference [1]. Manuscript received xx, 2025. K. Han, K. Meng, and C. Masouros are with the Department of Electronic and Electrical Engineering, University College London, London, UK (emails: {kawon.han, kaitao.meng, c.masouros}@ucl.ac.uk).

Recent advancements in ISAC have predominantly focused on link-level design [7]–[10] and resource allocation strategies [11], [12] for single-node configurations. These systems typically employ monostatic radar sensing and single base-station (BS) communication services, offering the enhanced spectrum efficiency and the improved ISAC performance. On the other hand, the ultimate goal of the ISAC deployment in cellular systems is to enable networked sensing of an unprecedented scale. However, the increased network density causes challenges such as inter-node interference and resource congestion [13], [14]. Therefore, the exploitation of networked ISAC systems and cooperation of multiple cells has been emerging as a promising configuration of the future wireless system. Unlike single-node systems, networked ISAC involves multiple interconnected nodes or BSs that operate in adjacent locations, which provide cooperative gains that significantly enhance both communication and sensing capabilities [15], [16]. This cooperative approach facilitates enhanced spectral efficiency, broader communication and sensing coverage, and enhanced accuracy in target parameter estimation, unlocking a new opportunity in ISAC technology. Recent investigations into network-level ISAC systems have explored areas such as spatial resource allocation [17], cooperative cluster configurations [18], and antenna-to-BS allocation [19], demonstrating the performance benefits achievable through multi-node cooperation.

System-level architectures for cooperative and networked ISAC systems have been studied across various scenarios to explore the potential of distributed configurations for ISAC [20]–[27]. In [20], [21], the cooperation of active and passive sensing has been investigated, where sensing signals received at multiple receivers are used to localize targets, corresponding to distributed single-input multi-output (SIMO) radar. Although they leverage increased spatial diversity by distributed architectures, those systems cannot fully enjoy cooperative transmission gains for both communication and sensing. On the other hand, [22]–[24] considered sensing cooperation based on distributed multi-input single-output (MISO) systems, leveraging transmitted signals from multiple transmit nodes, which lack of considerations of receiver diversity to improve distributed sensing performance. Distributed architectures presented in [25]–[27] explore joint collaboration among multiple transmitters and receivers to estimate target locations while simultaneously serving communication users or mitigating inter-node interference. However, these works fall short of fully exploiting the potential gains distributed ISAC (D-ISAC) achievable through spatial diversity of distributed antenna arrays, because they exploit only parts of scattered signals as only bistatic sensing [25] or only monostatic sensing [26], [27].

While preliminary studies have investigated various levels of cooperation with distributed architectures, signal-level designs remain underdeveloped for cooperative ISAC systems. In terms of transmit beamforming designs, [20] focused solely on multi-static sensing with distributed receivers, neglecting the distributed transmission in D-ISAC. On the other hand, [28] investigated cooperative beamforming in distributed cloud radio access networks (C-RAN) integrated with rate-splitting multiple access (RSMA). Likewise, the work [25] proposed coordinated beamforming (CBF) for distributed sensing and multi-user communication, emphasizing inter-cell interference mitigation. Although these coordinated beamforming approaches mitigate inter-node interference induced by simultaneous signal transmission from multiple nodes, they cannot exploit the signal and/or power combining gain in the D-ISAC system.

On the other hand, D-ISAC systems that utilize joint transmission (JT) schemes by sharing the transmitted signals among cooperative nodes have been considered in [29]–[32], which further improves the cooperative gain compared to D-ISAC using coordinated beamforming. In [29], a beamforming design for multi-static sensing and JT coordinated multipoint (CoMP) communication has been investigated. Related works [30], [31] introduced a transmit beamforming approach for multi-input multi-output (MIMO) ISAC systems, coherently serving communication users with multiple access points. In multi-cell ISAC [32], both block- and symbol-level precoding designs with joint transmission CoMP have been considered. However, these systems employ the coherent cooperation with phase-level synchronization among distributed nodes, which is challenging to achieve in practice. Also, they do not take the target localization gain into account in the signaling design, which is the unique advantage of the use of distributed MIMO radar [33].

Although classical coordinated beamforming [34] and CoMP transmission [35] can significantly enhance cooperative communication performance compared to the single-cell system, these approaches do not fully exploit the sensing gains achievable through distributed MIMO radar. Prior works discussed above primarily consider the improvement of AOA measurement for networked sensing [30], [31], [36], focusing on only beamforming design for their transmit signaling. Interestingly, distributed radar sensing architectures harness time-of-flight (TOF) information from spatially diverse reflection links, offering substantial improvements in localization accuracy [33], [37], [38]. However, fully leveraging both AOA and TOF measurements requires advanced signal-level designs that go beyond conventional spatial beamforming. This highlights a critical gap in current research: the systematic properties and ISAC trade-offs unique to D-ISAC systems remain underexplored, particularly in the context of transmit signal design. The comparisons of state-of-the-art D-ISAC signaling design are provided in Table I.

Building on these observations, we recognize that the potential performance gains from exploiting distributed configurations remain constrained by current design approaches. Therefore, it is imperative to investigate the achievable D-ISAC performance gains by incorporating optimal ISAC signal designs that jointly optimize sensing and communication performance. Motivated by this need, this work proposes a novel transmit signal design framework for D-ISAC systems. We consider a MIMO orthogonal frequency division multiplexing (OFDM)-based noncoherent D-ISAC system that operates without phase-level synchronization between nodes. While the performance gains of noncoherent cooperation may be limited compared to those of coherent systems, coherent cooperation requires not only accurate time-frequency synchronization but also phase alignment of spatially separated oscillators [39], which introduces excessive system complexity in distributed ISAC. Therefore, noncoherent systems are more practical for distributed wireless networks.

The proposed system comprises multiple ISAC nodes connected to a central processing unit (CPU) and employs CoMP transmission for multi-user communication. For sensing, it leverages both collocated and distributed MIMO radar configurations with monostatic and multistatic target links, utilizing AOA and TOF estimation to enhance target localization. Furthermore, low complexity of D-ISAC transmit signal design is crucial for practical implementation, particularly in distributed systems with large-scale configurations. To the best of our knowledge, this work is the first to establish a unified MIMO–OFDM based distributed ISAC signaling framework under noncoherent cooperation, which simultaneously addresses sensing accuracy, communication performance, and design complexity. The main contributions of this work are as follows:

- We propose a novel transmit signal design framework tailored for MIMO-OFDM D-ISAC systems. This integrates both collocated and distributed MIMO radar for target localization and noncoherent CoMP downlink communication. For the sensing functionality, a hybrid localization approach is employed, leveraging both AOA and TOF measurements, which enables precise target localization by combining the benefits of TOF- and AOA-based techniques.
- We develop a noncoherent D-ISAC signal model and establish performance metrics for multi-target sensing and multi-user communication. Subsequently, optimization problems are formulated to design MIMO-OFDM D-ISAC signals that minimize the noncoherent target localization Cramér-Rao bound (CRB) while ensuring a minimum signal-to-interference-plus-noise ratio (SINR) for communication users. We employ semidefinite relaxation (SDR) to solve the formulated non-convex problems.
- Three distinct transmit signal designs, including unconstrained, orthogonal, and beamforming designs, are introduced. The unconstrained design achieves the best sensing performance at the expense of computational complexity. The orthogonal design reduces computational requirements by ensuring inter-node signal orthogonality, while the beamforming design further simplifies implementation by focusing solely on optimizing AOA estimation performance. These designs are highly valuable for practical systems, offering flexible solutions that balance performance and

Table I
COMPARISONS OF STATE-OF-THE-ART DISTRIBUTED ISAC SIGNALING DESIGN

	[30]	[25]	[28]	[29]	[31]	[36]	**This work**
Multiple transmitters	✓	✓	✓	✓	✓	✓	✓
Multiple receivers	✓	✓	✓	✓	×	✓	✓
Multi-carrier waveform	×	×	×	×	×	×	✓
Phase-level synchronization	✓	×	✓	✓	✓	-	×
AOA optimization	✓	✓	✓	✓	✓	✓	✓
TOF optimization	×	×	×	×	×	×	✓
Cooperative communication	CoMP	CBF	RSMA	CoMP	CoMP	-	CoMP
Sensing performance metric	SNR	CRB	CRB	Beampattern	SINR	CRB	CRB

complexity in D-ISAC systems.

Extensive numerical simulations validate the proposed signal designs, demonstrating D-ISAC trade-off performance bounds and assessing the impact of key system parameters, such as signal bandwidth, the number of antennas, and the number of cooperative nodes. Additionally, the analysis explores the performance-complexity trade-offs among the three proposed designs.

Notations: Boldface variables with lower- and upper-case symbols represent vectors and matrices, respectively. $\mathbf{A} \in \mathbb{C}^{N\times M}$ and $\mathbf{B} \in \mathbb{R}^{N\times M}$ denotes a complex-valued $N\times M$ matrix $\mathbf{A}$ and a real-valued $N\times M$ matrix $\mathbf{B}$, respectively. Also, $\mathbf{0}_{N\times M}$ and $\mathbf{I}_N$ denote a $N\times M$ zero-matrix and a $N\times N$ identity matrix, respectively. $(\cdot)^T$, $(\cdot)^H$, and $(\cdot)^*$ represent the transpose, Hermitian transpose, and conjugate operators, respectively. $\mathrm{diag}(\mathbf{a})$ denotes a diagonal matrix with diagonal entries of a vector $\mathbf{a}$. $\odot$, $\bullet$, $*$, and $\otimes$ represent the Hadamard (element-wise) product, the Khatri-Rao product, the face-splitting product, and the Kronecker product, respectively. $\mathbb{E}[\cdot]$ is the statistical expectation operator.

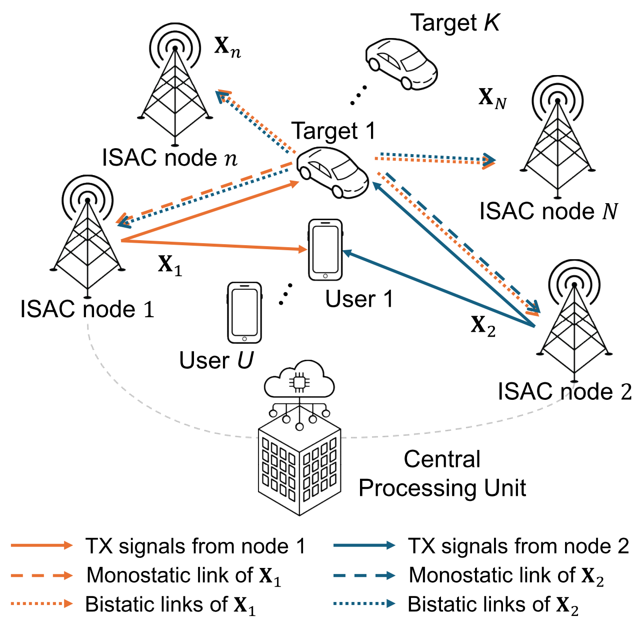

Fig. 1. Illustration of the D-ISAC system, where each ISAC node is equipped with both transmit and receive antenna arrays. Signals from other nodes are omitted for clarity. The D-ISAC system leverages all possible monostatic and bistatic links for target localization.

II. SYSTEM MODEL

A. Distributed ISAC System

In the proposed D-ISAC system, we integrate noncoherent CoMP transmission for cooperative communication with a distributed MIMO radar framework that leverages both monostatic and bistatic sensing. The noncoherent operation introduces a novel trade-off between communication and sensing performance. Using a distributed MIMO radar to jointly exploit monostatic and bistatic scattering for target localization, the system improves the sensing performance with ISAC networks given a communication performance, as illustrated in Fig. 1. To achieve this, all ISAC nodes are connected to a CPU, which is responsible for distributing communication data to each ISAC node and collecting radar-received signals for centralized fusion to estimate target parameters.

Each ISAC node is equipped with M_t transmit antennas and M_r receive antennas configured in a uniform linear array (ULA) with half-wavelength spacing. With N ISAC nodes, node n is located at $\mathbf{p}_n = [x_n, y_n]^T$ in a two-dimensional Cartesian coordinate system relative to the reference origin. Together, these networked ISAC nodes serve U single-antenna communication users and jointly detect K targets and estimate their corresponding parameters[1]. This cooperative operation enables the distributed ISAC network to handle communication and sensing tasks simultaneously. The D-ISAC system employs OFDM with L subcarriers over T time slots.

For simplicity, we assume that the transmit and receive antennas are deployed separately with sufficient isolation, making the self-interference caused by full-duplex operation negligible. Furthermore, the transmitted signals and channel state information (CSI) between ISAC nodes are shared and known in advance. This prior knowledge facilitates the cancellation of inter-node interference (INI) in the received signals by using interference nulling [18] and precoding design [40]. To ensure practical implementation, we consider a noncoherent cooperation framework, in which the ISAC nodes are synchronized in time and frequency but not in phase. We note that time-frequency synchronization is relatively straightforward

[1] It should be noted that all targets of interest are assumed to have been previously identified through a target-search process at the CPU. Accordingly, the sensing task in this work focuses on the localization of these associated targets.

and can be achieved to some extent using global positioning system (GPS) disciplined references [41]. On the other hand, phase synchronization is more difficult to achieve, because it requires aligning the instantaneous relative phases of distributed nodes that is highly sensitive to hardware-induced phase offset such as phase noises [42].

B. Transmit Signal Model

We introduce a weighted summation of multi-user communication and MIMO radar signals as the ISAC transmit waveform. The frequency-domain OFDM ISAC signal at a symbol index $t \in [1, 2, \cdots, T]$ is expressed as

$$\mathbf{X}_n[t] = \mathbf{X}_{c,n}[t] + \mathbf{X}_{s,n}[t], \tag{1}$$

where $\mathbf{X}_{c,n}[t] = \left[\mathbf{x}_{c,n,1}[t], \mathbf{x}_{c,n,2}[t], \cdots, \mathbf{x}_{c,n,L}[t]\right] \in \mathbb{C}^{M_t \times L}$, and the l^{th} column vector of $\mathbf{X}_{c,n}[t]$, representing the l^{th} subcarrier signal, is expressed as $\mathbf{x}_{c,n,l}[t] = \mathbf{W}_{c,n,l}\mathbf{s}_{c,l}[t] \in \mathbb{C}^{M_t \times 1}$. Here, $\mathbf{W}_{c,n,l} \in \mathbb{C}^{M_t \times U}$ is the precoding matrix for multi-user communication, and $\mathbf{s}_{c,l}[t] \in \mathbb{C}^{U \times 1}$ is the corresponding data symbol vector. Furthermore, $\mathbf{X}_{s,n}[t] \in \mathbb{C}^{M_t \times L}$ represents the radar signals at the ISAC node n. The power of communication and sensing signals is encapsulated in $\mathbf{X}_{c,n}[t]$ and $\mathbf{X}_{s,n}[t]$, respectively. Although a cyclic prefix (CP) is utilized to avoid inter-symbol interference (ISI), it is omitted in this formulation because the CP is removed during receiver processing at both the communication and radar receivers [43]. Its effect is embedded into the OFDM symbol as a phase rotation.

Without loss of generality, we assume that the communication symbols are random with zero mean and uncorrelated with the radar signals, ensuring

$$\mathbb{E}\left[\mathbf{x}_{c,n,l}[t]\mathbf{x}_{s,m,l}^H[t]\right] = \mathbf{0}_{M_t \times M_t}, \quad \forall n, m, \text{and } l. \tag{2}$$

Additionally, the modulated communication symbols for different users are uncorrelated, i.e.,

$$\mathbb{E}\left[\mathbf{s}_{c,l}[t]\mathbf{s}_{c,l}^H[t]\right] = \mathbf{I}_U, \quad \forall l. \tag{3}$$

For simplicity, we omit the symbol index t in the following discussions. Based on this transmit signal model, the goal is to design the D-ISAC transmit signal $\mathbf{X}_n, \forall n = 1, 2, \ldots, N$ to meet the desired system performance requirements. Alternatively, this can be viewed as jointly designing the communication precoders $\mathbf{W}_{c,n}$ for multi-user CoMP transmission and the distributed MIMO radar signals $\mathbf{X}_{s,n}$, while balancing their respective signal powers to optimize the trade-off between sensing and communication performance.

C. Communication Signal Model

According to the system description, each ISAC node transmits a dual-functional signal for radar sensing and downlink CoMP communication. Let $y_{c,u,l}$ denote the received OFDM signal on the l^{th} subcarrier at user u in the frequency domain, which is expressed as

$$\begin{aligned} y_{c,u,l} &= \sum_{n=1}^{N} \mathbf{h}_{n,u,l}^H \mathbf{x}_{n,l} + z_{c,u,l}, \\ &= \sum_{n=1}^{N} (\mathbf{h}_{n,u,l}^H \mathbf{w}_{c,n,u,l} s_{c,u,l} + \sum_{i=1, i \neq u}^{U} \mathbf{h}_{n,u,l}^H \mathbf{w}_{c,n,i,l} s_{c,i,l}) \\ &\quad + \sum_{n=1}^{N} \mathbf{h}_{n,u,l}^H \mathbf{x}_{s,n,l} + z_{c,u,l}, \end{aligned} \tag{4}$$

where $\mathbf{h}_{n,u,l}^H$ represents the channel impulse response for the l^{th} subcarrier between user u and ISAC node n. The term $z_{c,u,l}$ represents zero-mean complex-valued additive white Gaussian noise (AWGN), following with $z_{c,u,l} \sim \mathcal{CN}(0, \sigma_c^2/L)$. In our system model, we consider an inter-carrier interference (ICI)-free scenario. As shown in (4), the received communication signal is impacted by multi-user interference as well as radar signal interference transmitted from all cooperative ISAC nodes. Therefore, the communication SINR for noncoherent CoMP accounts for these interference components.

D. Sensing Signal Model

For multiple ISAC nodes, the received signal at each node includes both monostatic and bistatic scatterings from K targets. The received sensing signal at the n^{th} ISAC node, transmitted from the m^{th} node, is expressed as

$$\mathbf{Y}_{s,n,m} = \sum_{k=1}^{K} b_{n,m}^k \mathbf{a}_r(\theta_n^k) \left(\mathbf{a}_t^T(\theta_m^k)\mathbf{X}_m \odot \mathbf{d}^T(\tau_{n,m}^k)\right), \tag{5}$$

where $\mathbf{a}_r(\theta) \in \mathbb{C}^{M_r \times 1}$ and $\mathbf{a}_t(\theta) \in \mathbb{C}^{M_t \times 1}$ are the receive and transmit steering vectors, respectively, and $\mathbf{d}(\tau) \in \mathbb{C}^{L \times 1}$ represents the delay steering vector. These are defined as $\mathbf{a}_r(\theta) = \left[1, e^{j\frac{2\pi}{\lambda}d_0 \sin\theta}, \ldots, e^{j\frac{2\pi}{\lambda}(M_r-1)d_0 \sin\theta}\right]^T$, $\mathbf{a}_t(\theta) = \left[1, e^{j\frac{2\pi}{\lambda}d_0 \sin\theta}, \ldots, e^{j\frac{2\pi}{\lambda}(M_t-1)d_0 \sin\theta}\right]^T$, $\mathbf{d}(\tau) = \left[1, e^{-j2\pi\frac{B}{L}\tau}, e^{-j2\pi\frac{B}{L}2\tau}, \ldots, e^{-j2\pi\frac{B}{L}(L-1)\tau}\right]^T$, where λ is the wavelength, B is the signal bandwidth, and L is the number of subcarriers. Additionally, $b_{n,m}^k$ is the complex amplitude including target radar cross-section (RCS) and path-loss corresponding to target-to-node distance, and $\tau_{n,m}^k = \tau_n^k + \tau_m^k$ is the time-of-flight (TOF) from the m^{th} node to the k^{th} target and then to the n^{th} node. θ_n^k represents the angle of the target as seen from the n^{th} node. Let $\mathbf{q}_k = [x_k, y_k]^T$ denote the position of target k. Then, the TOF and angle are functions of the target location, given by $\tau_n^k = \frac{\sqrt{(x_k-x_n)^2+(y_k-y_n)^2}}{c}$, $\theta_n^k = \arctan 2(y_k - y_n, x_k - x_n)$, where c is the speed of light.

From (5), the received signal at node n is rewritten as

$$\begin{aligned} \mathbf{Y}_{s,n} &= \sum_{m=1}^{N} \left(\mathbf{A}_{r,n}\mathbf{B}_{n,m}\left(\mathbf{A}_{t,m}^T\mathbf{X}_m \odot \mathbf{D}_{n,m}^T\right)\right) + \mathbf{Z}_{s,n}, \\ &= \mathbf{A}_{r,n} \sum_{m=1}^{N} \left(\mathbf{B}_{n,m}\mathbf{V}_{n,m}^T\right) + \mathbf{Z}_{s,n}, \end{aligned} \tag{6}$$

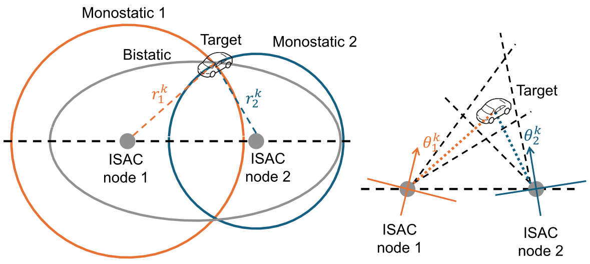

Fig. 2. Target localization methods in D-ISAC: (a) TOF-based localization and (b) AOA-based localization. The hybrid localization method combines TOF and AOA estimates to determine the target locations in the x-y coordinates.

where $\mathbf{V}_{n,m} = \mathbf{X}_m^T \mathbf{A}_{t,m} \odot \mathbf{D}_{n,m}$. The array, range, target amplitude matrices are given as $\mathbf{A}_{r,n} = \left[\mathbf{a}_r(\theta_n^1), \ldots, \mathbf{a}_r(\theta_n^K)\right]$, $\mathbf{A}_{t,n} = \left[\mathbf{a}_t(\theta_n^1), \ldots, \mathbf{a}_t(\theta_n^K)\right]$, $\mathbf{D}_{n,m} = \left[\mathbf{d}(\tau_{n,m}^1), \ldots, \mathbf{d}(\tau_{n,m}^K)\right]$, and $\mathbf{B}_{n,m} = \mathrm{diag}(b_{n,m}^1, \ldots, b_{n,m}^K)$. $\mathbf{Z}_{s,n}$ represents circularly symmetric complex Gaussian noise, where each entry follows $z_{s,n,i,j} \sim \mathcal{CN}(0, \sigma_n^2), \forall i \in \{1, ..., M_r\}, \forall j \in \{1, ..., L\}$. For notational simplicity and without loss of generality, we assume all nodes have the same noise variance, $\sigma_n^2 = \sigma_s^2/L$. Consequently, the sensing task in the D-ISAC system is to estimate the target locations $\mathbf{q}_k$ using the collected signals from all nodes, expressed as $\mathbf{Y}_s = [\mathbf{Y}_{s,1}^T, \mathbf{Y}_{s,2}^T, \ldots, \mathbf{Y}_{s,N}^T]^T$.

E. Target Localization Methods in D-ISAC

We focus on estimating the x-y locations of targets as the sensing task. To achieve this, it is essential to determine which measurements are utilized during receiver processing. Fig. 2 illustrates two types of target localization methods in the proposed D-ISAC system, of which details are as follows.

1) TOF-Based Localization: TOF-based localization relies solely on TOF measurements, a widely adopted approach in distributed MIMO radar [33], [44]. In the proposed fully active D-ISAC system, both monostatic and bistatic target links are available, enabling the extraction of TOF information for all links, as shown in Fig. 2(a). For this method, AOA information embedded in the signal model (6) is not utilized, making it equivalent to a distributed system with a single receive antenna per node or a system that performs TOF estimation after receiver beamforming toward the desired target direction. Consequently, angular information is not treated as an unknown parameter for estimation. This approach is particularly effective when the system operates with a large signal bandwidth, which enables high-resolution TOF measurements for precise localization. Moreover, the TOF-based localization accuracy follows the scaling law $\frac{1}{\ln^2 N}$, as reported in [19].

2) AOA-Based Localization: The D-ISAC system can also incorporate AOA information for target localization, as discussed in [28], [45]. In the proposed full-duplex D-ISAC system, the angle-of-departure (AOD) at the n^{th} node is identical to its AOA. As shown in Fig. 2(b), AOA-based localization estimates target angles relative to each node and translates them into x-y coordinates. This receiver processing is achieved by estimating AOA after range compression, which fixes the delay corresponding to the target range. As a result, the TOF information embedded in the received signal is not utilized for localization. Similar to TOF-based localization, AOA-based localization provides accurate results when the array aperture of each ISAC node is relatively large with the scaling law of $\frac{1}{\ln N}$ [19].

3) Hybrid Localization: The hybrid localization method leverages both TOF and AOA measurements to localize the target. This approach combines TOF- and AOA-based localization methods and is achieved by directly estimating the target locations $\mathbf{q}_k$ without separating TOF and AOA measurements.

III. Performance Metric for Distributed ISAC

A. Communication Performance Metric

For noncoherent D-ISAC transmission, we exploit signal-to-interference-plus-noise ratio (SINR) as communication performance metric for D-ISAC signal design. From (4), we develop SINR of the typical user u in the case of the noncoherent cooperation of the distributed ISAC system. Since the D-ISAC nodes are not phase-synchronized, the received signal at the typical communication user is a noncoherently combined signal of the jointly transmitted communication signals. The CP length has to be properly chosen to ensure ISI-free bistatic sensing between ISAC nodes, which also ensures an ISI-free CoMP transmission region for D-ISAC cooperation.

Accordingly, based on the received signal model, the SINR of the l^{th} subcarrier of u communication user can be developed as

$$\gamma_{c,u,l} = \frac{\sum_{n=1}^{N} |\mathbf{h}_{n,u,l}^H \mathbf{w}_{c,n,u,l}|^2}{\sum_{n=1}^{N} \left[\sum_{i=1, i\neq u}^{U} |\mathbf{h}_{n,u,l}^H \mathbf{w}_{c,n,i,l}|^2 + |\mathbf{h}_{n,u,l}^H \mathbf{x}_{s,n,l}|^2\right] + \sigma_c^2/L}. \tag{7}$$

Note that the classical SINR expression in a coherent transmission scheme is represented as the square of the sum of all transmitted signals from N nodes. This arises because the phase coherence among the transmitting nodes is preserved, resulting in the received signals being coherently combined.

In contrast, for the noncoherent D-ISAC, the useful communication signals transmitted by the cooperative ISAC nodes are noncoherently combined at the user receiver, implying power combining of multiple transmitted signals. Also, it can be easily observed that the transmitted sensing signals and multi-user interference from all ISAC nodes are noncoherently added together, contributing to the increase of interference power. Consequently, the SINR at the typical communication user is represented as the sum of the squared values of the transmitted signals from multiple ISAC nodes. One may refer to [46] for the detailed proof of the SINR derivation.

B. Sensing Performance Metric

For a sensing performance metric, we exploit CRB of target localization in the cooperative ISAC nodes. Let $\mathbf{\Psi}$ denote the collection of all the real-valued unknown parameters given as

$$\mathbf{\Psi} = [\boldsymbol{\theta}^T, \boldsymbol{\tau}^T, \mathbf{b}_{\mathrm{R}}^T, \mathbf{b}_{\mathrm{I}}^T]^T \in \mathbb{R}^{(2KN+2KN^2)\times 1}, \tag{8}$$

where $\boldsymbol{\theta} = [\theta_1^1, \theta_1^2, \ldots, \theta_n^k, \ldots, \theta_N^K]^T \in \mathbb{R}^{KN\times 1}$, $\boldsymbol{\tau} = [\tau_1^1, \tau_1^2, \ldots, \tau_n^k, \ldots, \tau_N^K]^T \in \mathbb{R}^{KN\times 1}$, $\mathbf{b} = [b_{1,1}^1, b_{1,1}^2, \ldots, b_{n,i}^k, \ldots, b_{N,N}^K]^T \in \mathbb{C}^{KN^2\times 1}$, and $\mathbf{b}_{\mathrm{R}} = \mathrm{Re}(\mathbf{b}), \mathbf{b}_{\mathrm{I}} = \mathrm{Im}(\mathbf{b})$. Since both $\boldsymbol{\theta}$ and $\boldsymbol{\tau}$ contribute to localize targets in Cartesian coordination, we can alternatively define the vector of unknown parameter as

$$\boldsymbol{\Theta} = [\mathbf{x}^T, \mathbf{y}^T, \mathbf{b}_{\mathrm{R}}^T, \mathbf{b}_{\mathrm{I}}^T]^T \in \mathbb{R}^{(2KN^2+2K)\times 1}, \quad (9)$$

where $\mathbf{x} = [x_1, x_2, \ldots, x_K]^T \in \mathbb{R}^{K\times 1}$ and $\mathbf{y} = [y_1, y_2, \ldots, y_K]^T \in \mathbb{R}^{K\times 1}$.

The joint log-likelihood function of the observation $\mathbf{Y}_s$ conditioned on $\boldsymbol{\Psi}$ is given by [33]

$$\mathcal{L}(\mathbf{Y}_s|\boldsymbol{\Psi}) = -\sum_{n=1}^{N} \left\| \mathbf{Y}_{s,n} - \mathbf{A}_{r,n} \sum_{m=1}^{N} \left(\mathbf{B}_{n,m} \mathbf{V}_{n,m}^T \right) \right\|_F^2 + c_0, \quad (10)$$

where c_0 is some constant. Then, the Fisher Information matrix (FIM) with respect to $\boldsymbol{\Psi}$ is expressed as

$$\mathbf{F}(\boldsymbol{\Psi}) = \mathbb{E}\left[\left(\frac{\partial}{\partial \boldsymbol{\Psi}} \mathcal{L}(\mathbf{Y}_s|\boldsymbol{\Psi}) \right) \left(\frac{\partial}{\partial \boldsymbol{\Psi}} \mathcal{L}(\mathbf{Y}_s|\boldsymbol{\Psi}) \right)^T \right]. \quad (11)$$

To obtain the FIM with respect to target localization parameters $\boldsymbol{\Theta}$, we adopt the chain rule as follows:

$$\mathbf{F}(\boldsymbol{\Theta}) = \mathbf{J}\mathbf{F}(\boldsymbol{\Psi})\mathbf{J}^T, \quad (12)$$

where $\mathbf{J}$ is the Jacobian matrix expressed as $\mathbf{J} = \frac{\partial \boldsymbol{\Psi}}{\partial \boldsymbol{\Theta}}$. Finally, we get the sensing metric related to the target localization CRB, which is expressed as

$$\mathrm{CRB} = \mathrm{tr}\left([\mathbf{F}(\boldsymbol{\Theta})]^{-1} \right). \quad (13)$$

In the case of a coherent distributed MIMO radar system with the phase-level synchronization, one can leverage additional information corresponding to TOFs embedded in the phase of the complex amplitude $\mathbf{b}$, which enables to have coherent distributed MIMO radar gain for target localization [33]. On the other hand, phase synchronization cannot be achieved between ISAC nodes for the noncoherent D-ISAC system, where the target complex amplitude $\mathbf{b}$ remains as nuisance parameters. Therefore, (8) and (11) are directly applied to get the FIM and the Jacobian matrix without any modification. The detailed derivation of the FIM $\mathbf{F}(\boldsymbol{\Psi})$ for noncoherent D-ISAC is developed in Appendix A.

IV. Distributed ISAC Signal Design

A. Problem Formulation

Unlike monostatic ISAC systems, where transmit signal design primarily focuses on dual-functional radar-communication (DFRC) beamforming [47], [48], the D-ISAC system requires a more advanced approach that considers signal design for optimal TOF estimation and inter-node signal correlation. In D-ISAC, target localization performance depends on both TOF and AOA metrics, necessitating a transmit signal design that explicitly accounts for these parameters. This underscores the limitation of DFRC beamforming alone in achieving optimal localization performance for D-ISAC systems, as it overlooks the integration of TOF measurements and the power allocation across multiple transmit nodes. To address these challenges, we develop a signal design framework that balances the trade-off between the target localization CRB and the CoMP communication SINR. Additionally, we propose three distinct D-ISAC signal design approaches: (1) unconstrained design, (2) orthogonal design, and (3) beamforming design. Each of these approaches demonstrates specific trade-offs between ISAC performance and computational complexity, allowing flexibility in system implementation depending on the performance requirements and resource constraints.

Using the communication and sensing performance metrics described in Sections III-A and III-B, the objective of the transmit signal design for noncoherent D-ISAC is to minimize the localization CRB while guaranteeing the communication SINR constraints for all downlink users. This can be generally formulated as the following optimization problem under a per-antenna power constraint:

$$\underset{\{\mathbf{X}_n\}}{\text{minimize}} \quad \mathrm{tr}\left([\mathbf{F}(\boldsymbol{\Theta})]^{-1} \right) \quad (14a)$$

$$\text{subject to} \quad [\mathbf{R}_n]_{m,m} \le P_T, \ \forall n, m, \quad (14b)$$

$$\gamma_{c,u,l} \ge \Gamma_c, \ \forall u, l, \quad (14c)$$

where $\mathbf{R}_n = \mathbb{E}[\mathbf{X}_n \mathbf{X}_n^H]$ represents the transmit covariance matrix for the n^{th} node. The objective function (14a) minimizes the localization CRB, which reflects the target localization performance of the distributed MIMO radar. The constraint (14b) imposes a per-antenna power constraint on all ISAC nodes, where n and m denote the node and antenna indices, respectively. The constraint (14c) ensures that the SINR for each user across all OFDM subcarriers meets the threshold Γ_c, which allows the sensing operation without jeopardizing the communication quality of service (QoS). The optimization problem (14) is non-convex due to the fractional structure of the objective function and quadratic constraints. Thus, we analyze and relax it into a convex problem using SDR. We explore three distinct signal designs and expand and tailor the above optimization to each of these, as described in the subsequent sections.

B. Unconstrained Signal Design ($\mathcal{P}$.1)

For the D-ISAC transmit signal design, we use SDR to solve problem (14) without imposing any signaling constraint between ISAC signals transmitted from different nodes. A radar waveform utilizing subcarrier-by-subcarrier signaling, $\mathbf{X}_{s,n} = [\mathbf{x}_{s,n,1}, \ldots, \mathbf{x}_{s,n,L}]$, is introduced, where each vector is defined as

$$\mathbf{x}_{s,n,l} = \mathbf{W}_{s,n,l}\mathbf{s}_{s,l}, \quad (15)$$

with $\mathbf{W}_{s,n,l}$ as a $M_t \times M_t$ matrix and $\mathbf{s}_{s,l}$ as a $M_t \times 1$ radar signal column vector. Consistent with (3), we adopt uncorrelated radar sequences across transmit antennas in the same ISAC node, satisfying $\mathbb{E}[\mathbf{s}_{s,l}\mathbf{s}_{s,l}^H] = \mathbf{I}_{M_t}, \forall l \in \{1, \ldots, L\}$. In the proposed unconstrained D-ISAC signal design, since no constraints are imposed on ISAC signals between different nodes, there is no condition on $\mathbb{E}[\mathbf{x}_{n,l}\mathbf{x}_{m,l}^H], \forall n \ne m$. Cross-correlations of the signals between nodes are encapsulated in $\mathbf{W}_{n,l}\mathbf{W}_{m,l}^H$, where $\mathbf{W}_{n,l} = [\mathbf{W}_{c,n,l}, \mathbf{W}_{s,n,l}]$.

We first examine the FIM for target localization. By observing each block matrix of the FIM, each submatrix of $\mathbf{F}$ includes the products of $\mathbf{V}$, $\dot{\mathbf{V}}_\theta$, and $\dot{\mathbf{V}}_\tau$, with the node indices

This article has been accepted for publication in IEEE Transactions on Wireless Communications. This is the author's version which has not been fully edited and content may change prior to final publication. Citation information: DOI 10.1109/TWC.2025.3633615

n and m omitted. The following lemma and theorem are then used to recast the quadratic constraint of problem (14) into a linear expression.

Lemma 1. *Any product of* $\mathbf{V}$*,* $\dot{\mathbf{V}}_\theta$*, and* $\dot{\mathbf{V}}_\tau$ *can be expressed in the following form:*

$$\mathbf{V}_{n,i}^H \mathbf{V}_{n,j} = (\mathbf{A}_{t,i} * \mathbf{D}_{n,i})^H (\mathbf{X}_i^* * \mathbf{I}_L)(\mathbf{X}_j * \mathbf{I}_L)^T (\mathbf{A}_{t,j} * \mathbf{D}_{n,j}), \quad (16)$$

Proof. This result is readily derived using the face product property $(\mathbf{AC}) \odot (\mathbf{BD}) = (\mathbf{A} \bullet \mathbf{B})(\mathbf{C} * \mathbf{D}) = (\mathbf{A}^T * \mathbf{B}^T)(\mathbf{C} * \mathbf{D})$ [49]. ■

Let $\tilde{\mathbf{x}}_l$ denote the l^{th} column of $\tilde{\mathbf{X}}$, where $\tilde{\mathbf{X}} = \left[\mathbf{X}_1^T, \mathbf{X}_2^T, \ldots, \mathbf{X}_N^T\right]^T$ is the augmented transmit signal matrix. By defining $\tilde{\mathbf{R}}_l = \mathbb{E}[\tilde{\mathbf{x}}_l \tilde{\mathbf{x}}_l^H]$, the following theorem provides insights for the FIM with respect to the D-ISAC transmit signal.

Theorem 1. *The FIM* $\mathbf{F}$ *for target localization in the noncoherent D-ISAC is a linear function of* $\tilde{\mathbf{R}}_l^T, \forall l \in \{1, 2, \ldots, L\}$.

Proof. From Lemma 1, $\mathbf{V}_{n,i}^H \mathbf{V}_{n,j}$ is a function of $(\mathbf{X}_i^* * \mathbf{I}_L)(\mathbf{X}_j * \mathbf{I}_L)^T$, which can be rewritten as

$$\begin{aligned}(\mathbf{X}_i^* * \mathbf{I}_L)(\mathbf{X}_j * \mathbf{I}_L)^T &= \sum_{l=1}^{L} (\mathbf{x}_{i,l}^* \otimes \mathbf{e}_l)(\mathbf{x}_{j,l}^T \otimes \mathbf{e}_l^T) \\ &= \sum_{l=1}^{L} (\mathbf{x}_{i,l}^* \mathbf{x}_{j,l}^T) \otimes (\mathbf{e}_l \mathbf{e}_l^T). \quad (17)\end{aligned}$$

Clearly, $\mathbb{E}[\mathbf{V}_{n,i}^H \mathbf{V}_{n,j}]$ is a linear function of $\mathbf{R}_{ij,l}^T = \mathbb{E}[\mathbf{x}_{i,l}^* \mathbf{x}_{j,l}^T], \forall l \in \{1, 2, \ldots, L\}$. Then, we have

$$\mathbf{R}_{ij,l} = \mathbf{W}_{c,i,l} \mathbf{W}_{c,j,l}^H + \mathbf{W}_{s,i,l} \mathbf{W}_{s,j,l}^H. \quad (18)$$

Since the FIM includes $\mathbb{E}[\mathbf{V}_{n,i}^H \mathbf{V}_{n,j}], \forall i, j \in \{1, 2, \ldots, N\}$, it is also a linear function of $\mathbf{R}_{ij,l}^T, \forall i, j \in \{1, 2, \ldots, N\}$, and $\forall l \in \{1, 2, \ldots, L\}$.

Defining the augmented communication precoding matrix $\tilde{\mathbf{W}}_{c,l} = [\mathbf{W}_{c,1,l}^T, \ldots, \mathbf{W}_{c,N,l}^T]^T \in \mathbb{C}^{M_t N \times U}$, the augmented sensing signal matrix $\tilde{\mathbf{W}}_{s,l} = [\mathbf{W}_{s,1,l}^T, \ldots, \mathbf{W}_{s,N,l}^T]^T \in \mathbb{C}^{M_t N \times M_t N}$, and $\tilde{\mathbf{W}}_l = [\tilde{\mathbf{W}}_{c,l}, \tilde{\mathbf{W}}_{s,l}] \in \mathbb{C}^{M_t N \times (U + M_t)}$ for the l^{th} subcarrier, $\tilde{\mathbf{R}}_l = \mathbb{E}[\tilde{\mathbf{x}}_l \tilde{\mathbf{x}}_l^H]$ is expressed as

$$\begin{aligned}\tilde{\mathbf{R}}_l &= \tilde{\mathbf{W}}_{c,l} \tilde{\mathbf{W}}_{c,l}^H + \tilde{\mathbf{W}}_{s,l} \tilde{\mathbf{W}}_{s,l}^H \\ &= \sum_{u=1}^{U} \tilde{\mathbf{w}}_{c,u,l} \tilde{\mathbf{w}}_{c,u,l}^H + \tilde{\mathbf{W}}_{s,l} \tilde{\mathbf{W}}_{s,l}^H, \\ &= \sum_{u=1}^{U} \tilde{\mathbf{R}}_{c,u,l} + \tilde{\mathbf{R}}_{s,l}, \quad (19)\end{aligned}$$

where $\tilde{\mathbf{w}}_{c,u,l}$ is the u^{th} column of $\tilde{\mathbf{W}}_{c,l}$, $\tilde{\mathbf{R}}_{c,u,l} = \tilde{\mathbf{w}}_{c,u,l} \tilde{\mathbf{w}}_{c,u,l}^H$, and $\tilde{\mathbf{R}}_{s,l} = \tilde{\mathbf{W}}_{s,l} \tilde{\mathbf{W}}_{s,l}^H$. Equivalently, $\tilde{\mathbf{R}}_l$ can be represented as the following block matrix:

$$\tilde{\mathbf{R}}_l = \begin{bmatrix} \mathbf{R}_{11,l} & \mathbf{R}_{12,l} & \cdots & \mathbf{R}_{1N,l} \\ \mathbf{R}_{21,l} & \mathbf{R}_{22,l} & \cdots & \mathbf{R}_{2N,l} \\ \vdots & \vdots & \ddots & \vdots \\ \mathbf{R}_{N1,l} & \mathbf{R}_{N2,l} & \cdots & \mathbf{R}_{NN,l} \end{bmatrix} \in \mathbb{C}^{M_t N \times M_t N}. \quad (20)$$

Accordingly, the FIM is a linear function of $\tilde{\mathbf{R}}_l$, and this thus completes the proof. ■

Remark 1: Theorem 1 provides some insights on the performance of the proposed D-ISAC system. Unlike a single-node ISAC transmit signal design, we can leverage a hybrid of TOF and AOA information for the target localization in D-ISAC. Since the estimation of TOF is performed along the subcarrier-axis, i.e. $l = \{1, 2, \cdots, L\}$, per-subcarrier sensing signal design is required to optimize the localization accuracy.

We now rewrite the communication SINR for noncoherent CoMP in (7) to relax the quadratic constraint (14c). The diagonal submatrix of $\tilde{\mathbf{R}}_l$, denoted as $\mathbf{R}_{nn,l}$, $\forall n, l$, can be written as

$$\begin{aligned}\mathbf{R}_{nn,l} &= \sum_{u=1}^{U} \mathbf{w}_{c,n,u,l} \mathbf{w}_{c,n,u,l}^H + \mathbf{W}_{s,n,l} \mathbf{W}_{s,n,l}^H \\ &= \sum_{u=1}^{U} \mathbf{R}_{c,n,u,l} + \mathbf{R}_{s,n,l}, \quad (21)\end{aligned}$$

where $\mathbf{R}_{c,n,u,l} = \mathbf{w}_{c,n,u,l} \mathbf{w}_{c,n,u,l}^H$ is rank-one. Using (21), the communication SINR in (7) can be expressed as

$$\gamma_{c,u,l} = \frac{\sum_{n=1}^{N} \mathbf{h}_{n,u,l}^H \mathbf{R}_{c,n,u,l} \mathbf{h}_{n,u,l}}{\sum_{n=1}^{N} \mathbf{h}_{n,u,l}^H (\mathbf{R}_{nn,l} - \mathbf{R}_{c,n,u,l}) \mathbf{h}_{n,u,l} + \sigma_c^2 / L}. \quad (22)$$

Since $\mathbf{R}_{s,n,l}$ is encapsulated in $\mathbf{R}_{nn,l}$, the communication SINR is a linear constraint with respect to $\mathbf{R}_{nn,l}$ and $\mathbf{R}_{c,n,u,l}$.

By adopting Theorem 1 and substituting (22) into the problem (14), we reformulate the problem (14) in an equivalent form using the Schur complement as follows [50]:

$$\underset{\{\tilde{\mathbf{R}}_{c,u,l}\}, \{\tilde{\mathbf{R}}_l\}}{\text{minimize}} \quad \sum_{i=1}^{2K} t_i \quad (23a)$$

$$\text{subject to} \quad \begin{bmatrix} \mathbf{F} & \mathbf{e}_i \\ \mathbf{e}_i^T & t_i \end{bmatrix} \succeq 0, \ \forall i \in \{1, \ldots, 2K + 2KN^2\}, \quad (23b)$$

$$[\tilde{\mathbf{R}}]_{m,m} \leq P_T, \ \forall m, \quad (23c)$$

$$\tilde{\mathbf{R}}_{c,u,l} \succeq 0, \ \text{rank}(\tilde{\mathbf{R}}_{c,u,l}) = 1, \forall u, l, \quad (23d)$$

$$\tilde{\mathbf{R}}_l - \sum_{u=1}^{U} \tilde{\mathbf{R}}_{c,u,l} \succeq 0, \forall u, l \quad (23e)$$

$$\sum_{n=1}^{N} \left[\left(1 + \frac{1}{\Gamma_c}\right) \mathbf{h}_{n,u,l}^H \mathbf{R}_{c,n,u,l} \mathbf{h}_{n,u,l} - \mathbf{h}_{n,u,l}^H \mathbf{R}_{nn,l} \mathbf{h}_{n,u,l} \right] \geq \frac{\sigma_c^2}{L}, \quad (23f)$$

where $\mathbf{e}_i$ is the i^{th} column of the identity matrix $\mathbf{I}_{(2K+2KN^2)}$, and $\mathbf{F}$ denotes the FIM matrix, simplified for brevity. Similar to the notation, where $\mathbf{R}_{nn,l}$ is a diagonal submatrix of $\tilde{\mathbf{R}}_l$, here $\mathbf{R}_{c,n,u,l}$ is also a diagonal submatrix of $\tilde{\mathbf{R}}_{c,u,l}$. The constraint (23c) addresses the per-antenna power constraint, where $\forall m \in \{1, 2, \cdots, NM_t\}$ with $\tilde{\mathbf{R}} = \sum_{l=1}^{L} \tilde{\mathbf{R}}_l$. The constraints (23d)–(23f) hold $\forall u \in \{1, \cdots, U\}$ and $\forall l \in \{1, \cdots, L\}$.

Remark 2: Here, one can observe that off-diagonal submatrices of $\tilde{\mathbf{R}}_l$ have no effects on the communication SINR constraint (23f). This is because the noncoherent CoMP leverages a power combining gain without phase coherency, implying that the cross-correlation between different nodes does not contribute to the received signal power at a typical communication user. Accordingly, we can simplify the problem by neglecting off-diagonal submatrics of $\tilde{\mathbf{R}}_{c,u,l}$.

This article has been accepted for publication in IEEE Transactions on Wireless Communications. This is the author's version which has not been fully edited and content may change prior to final publication. Citation information: DOI 10.1109/TWC.2025.3633615

Dropping the rank-one constraint out, we recast (23) as a semidefinite programming (SDP) problem:

$$(\mathcal{P}.1)\ \underset{\{\mathbf{R}_{c,n,u,l}\},\{\tilde{\mathbf{R}}_l\}}{\text{minimize}} \quad \sum_{i=1}^{2K} t_i \tag{24a}$$

$$\text{subject to} \quad \text{(23b), (23c), and (23f)} \tag{24b}$$

$$\mathbf{R}_{c,n,u,l} \succeq 0,\ \tilde{\mathbf{R}}_l \succeq 0, \forall n,u,l, \tag{24c}$$

$$\mathbf{R}_{nn,l} - \sum_{u=1}^{U} \mathbf{R}_{c,n,u,l} \succeq 0, \forall n,l, \tag{24d}$$

The formulated problem $(\mathcal{P}.1)$ is now a standard SDP, which can be solved via a CVX solver in polynomial time.

Although the relaxation to problem $(\mathcal{P}.1)$ is not necessarily tight, we can extract solutions for $\hat{\mathbf{w}}_{c,n,u,l}$ and $\hat{\mathbf{W}}_{s,n,l}$ from the obtained solutions $\mathbf{R}_{c,n,u,l}$ and $\tilde{\mathbf{R}}_l$ of the relaxed problem. First, the following theorem provides the existence of the solution $\mathbf{R}_{c,n,u,l}$ to (24) that satisfies $\text{rank}(\mathbf{R}_{c,n,u,l}) = 1$.

Theorem 2. *Let $\mathbf{R}_{nn,l}$ and $\mathbf{R}_{c,n,u,l}$ denote an optimal solution to problem* (24)*. Then,*

$$\tilde{\mathbf{R}}_{nn,l} = \mathbf{R}_{nn,l}, \tag{25}$$

$$\tilde{\mathbf{R}}_{c,n,u,l} = \frac{\mathbf{R}_{c,n,u,l}\boldsymbol{h}_{n,u,l}\boldsymbol{h}_{n,u,l}^H\mathbf{R}_{c,n,u,l}^H}{\boldsymbol{h}_{n,u,l}^H\mathbf{R}_{c,n,u,l}\boldsymbol{h}_{n,u,l}}, \tag{26}$$

also constitute an optimal solution, where rank($\tilde{\mathbf{R}}_{c,n,u,l}$)=1.

Proof. Please see Appendix B. ∎

Building on the above theorem, $\hat{\mathbf{w}}_{c,n,u,l}$ can be obtained from $\mathbf{R}_{c,n,u,l}$ as follows:

$$\hat{\mathbf{w}}_{c,n,u,l} = \left(\mathbf{h}_{n,u,l}^H\mathbf{R}_{c,n,u,l}\mathbf{h}_{n,u,l}\right)^{-1/2}\mathbf{R}_{c,n,u,l}\mathbf{h}_{n,u,l}. \tag{27}$$

Next, we construct the augmented communication precoding matrix $\widehat{\widetilde{\mathbf{W}}}_{c,l}$ using the obtained $\hat{\mathbf{w}}_{c,n,u,l}$. Then, the following covariance matrix of the radar signal can be constructed:

$$\widehat{\widetilde{\mathbf{R}}}_{s,l} = \tilde{\mathbf{R}}_l - \widehat{\widetilde{\mathbf{W}}}_{c,l}\widehat{\widetilde{\mathbf{W}}}_{c,l}^H. \tag{28}$$

However, $\widehat{\widetilde{\mathbf{R}}}_{s,l}$ cannot be directly decomposed into $\widehat{\widetilde{\mathbf{W}}}_{s,l}$. This is because the off-diagonal submatrices of $\widehat{\widetilde{\mathbf{R}}}_{s,l}$ are not necessarily positive semidefinite, while the diagonal submatrices are positive semidefinite due to (24d). Therefore, we first project $\widehat{\widetilde{\mathbf{R}}}_{s,l}$ onto the positive semidefinite cone [51], and then apply the Cholesky decomposition or eigenvalue decomposition [52] to get

$$\widehat{\widetilde{\mathbf{W}}}_{s,l}\widehat{\widetilde{\mathbf{W}}}_{s,l}^H \approx \tilde{\mathbf{R}}_l - \widehat{\widetilde{\mathbf{W}}}_{c,l}\widehat{\widetilde{\mathbf{W}}}_{c,l}^H. \tag{29}$$

The obtained solutions are not necessarily optimal for the original problem (23), since the relaxation does not capture the contribution of the communication precoding matrix to the off-diagonal blocks of $\tilde{\mathbf{R}}_l$ and, moreover, it does not preserve the rank-one property of the augmented per-user communication covariances $\tilde{\mathbf{R}}_{c,u,l}$. Nevertheless, the extracted solutions can be used as feasible solutions for the unconstrained D-ISAC transmit signal design problem.

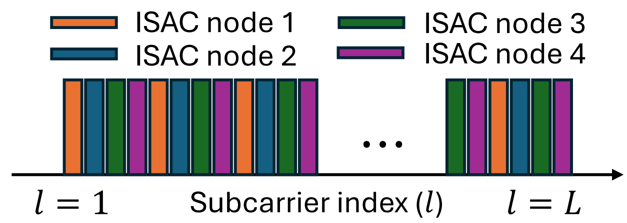

Fig. 3. Subcarrier-interleaving in OFDM D-ISAC signaling with orthogonal signal transmission when $N = 4$.

C. Orthogonal Signal Design $(\mathcal{P}.2)$

While the formulated problem $(\mathcal{P}.1)$ can provide convex relaxation bound for the optimal noncoherent D-ISAC performance, it incurs high computational complexity due to the large number of variables, which we analyze in Section IV-E. Importantly, the off-diagonal matrices of $\tilde{\mathbf{R}}_l$ are not relevant to the communication SINR constraint in (22). Moreover, orthogonal transmission enables distributed MIMO receivers to easily separate multistatic links, thereby exploiting spatial diversity for sensing tasks without requiring complex receiver processing [33]. Motivated by these observations, we propose a suboptimal, low-complexity D-ISAC signal design based on orthogonal signal transmission across ISAC nodes.

To ensure the orthogonality of signals $\mathbf{x}_{n,l}$ and $\mathbf{x}_{m,l}$, the subcarrier-interleaving approach is adopted, where the subcarriers for each ISAC node are allocated such that they do not overlap as shown in Fig. 3. Assuming the number of subcarriers is sufficiently larger than the number of ISAC nodes, i.e., $L \gg N$, the orthogonal signal model can be expressed as

$$\mathbf{x}_{n,l} = \begin{cases} \mathbf{W}_{c,n,l}\mathbf{s}_{c,l} + \mathbf{W}_{s,n,l}\mathbf{s}_{s,l}, & \text{if } n = l \text{ (mod } N), \\ \mathbf{0}_{M_t\times 1}, & \text{otherwise.} \end{cases} \tag{30}$$

This ensures that the cross-correlation between ISAC signals transmitted from different nodes is zero, irrespective of the sample number, i.e., $\mathbf{x}_{n,l}\mathbf{x}_{m,l}^H = \mathbf{0}_{M_t\times M_t}, \forall n \neq m$. By leveraging orthogonal signal transmission, the number of variables in the formulated problem can be significantly reduced compared to the case of the unconstrained signal design. This reduction is formalized in the following proposition. Hereafter, let us define the ISAC node index $\bar{n} = l$ (mod N), which serves the l^{th} subcarrier.

Proposition 1. *For the D-ISAC transmit signal with orthogonal signals, the FIM for target localization is a linear function of $\mathbf{R}_{\bar{n}\bar{n},l}, \forall(\bar{n},l) \in \{(\bar{n},l) \mid \bar{n} = l \text{ (mod } N), \forall l \in \{1,2,\ldots,L\}\}$.*

Proof. Based on (30), the ISAC signal of the l^{th} subcarrier is only present in the transmitted signal of the ISAC node $\bar{n}$, where $\bar{n} = l$ (mod N). Thus, off-diagonal submatrices of $\tilde{\mathbf{R}}_l$ are zero matrices, except for diagonal submatrices $\mathbf{R}_{\bar{n}\bar{n},l}$. ∎

We now reformulate the transmit signal design problem under the orthogonal signal condition based on Proposition 1. While the relaxation procedure remains the same as in the previous section, the variables are modified according to the

This article has been accepted for publication in IEEE Transactions on Wireless Communications. This is the author's version which has not been fully edited and content may change prior to final publication. Citation information: DOI 10.1109/TWC.2025.3633615

orthogonal signal model. The communication SINR in (22) is then updated as

$$\gamma_{c,u,l} = \frac{\mathbf{h}_{\bar{n},u,l}^H \mathbf{R}_{c,\bar{n},u,l} \mathbf{h}_{\bar{n},u,l}}{\mathbf{h}_{\bar{n},u,l}^H (\mathbf{R}_{\bar{n}\bar{n},l} - \mathbf{R}_{c,\bar{n},u,l}) \mathbf{h}_{\bar{n},u,l} + \sigma_c^2/L}. \tag{31}$$

Applying Proposition 1 and the updated SINR expression in (31), and dropping the rank-one constraint in (23), we formulate the relaxed problem for the D-ISAC transmit design with orthogonal signaling ($\mathcal{P}$.2) as

$$(\mathcal{P}.2) \underset{\{\mathbf{R}_{c,\bar{n},u,l}\},\{\mathbf{R}_{\bar{n}\bar{n},l}\}}{\text{minimize}} \quad \sum_{i=1}^{2K} t_i \tag{32a}$$

$$\text{subject to} \quad \text{(23b) and (23c)} \tag{32b}$$

$$\mathbf{R}_{c,\bar{n},u,l} \succeq 0, \ \forall \bar{n}, u, l, \tag{32c}$$

$$\mathbf{R}_{\bar{n}\bar{n},l} - \sum_{u=1}^{U} \mathbf{R}_{c,\bar{n},u,l} \succeq 0, \ \forall \bar{n}, l, \tag{32d}$$

$$\left(1 + \frac{1}{\Gamma_c}\right) \mathbf{h}_{\bar{n},u,l}^H \mathbf{R}_{c,\bar{n},u,l} \mathbf{h}_{\bar{n},u,l} - \mathbf{h}_{\bar{n},u,l}^H \mathbf{R}_{\bar{n}\bar{n},l} \mathbf{h}_{\bar{n},u,l} \geq \frac{\sigma_c^2}{L}, \tag{32e}$$

Here, the constraints (32c)–(32e) hold for $\forall(\bar{n}, l) \in \{(\bar{n}, l) \mid \bar{n} = l \pmod{N}, \forall l \in \{1, 2, \ldots, L\}\}$ and $\forall u \in \{1, \ldots, U\}$. The formulated problem ($\mathcal{P}$.2) is a convex problem, which can be solved using a CVX solver. Compared to the unconstrained signal design problem ($\mathcal{P}$.1), the number of variables in ($\mathcal{P}$.2) is significantly reduced, which will be further analyzed in Section IV-E.

To extract the solution of $\hat{\mathbf{w}}_{c,\bar{n},u,l}$ and $\hat{\mathbf{W}}_{s,\bar{n},l}$, we exploit a similar approach as in (27)–(29). Notably, the optimal solution of the original problem (14) under orthogonal signal transmission can be derived from the optimal solution of ($\mathcal{P}$.2), as supported by the following theorem.

Theorem 3. *Given that $\mathbf{R}_{c,\bar{n},u,l}$ and $\mathbf{R}_{\bar{n}\bar{n},l}$ are the optimal solutions of the relaxed problem ($\mathcal{P}$.2), the following extracted solutions $\hat{\mathbf{w}}_{c,\bar{n},u,l}$ and $\hat{\mathbf{W}}_{s,\bar{n},l}$, expressed as*

$$\hat{\mathbf{w}}_{c,\bar{n},u,l} = \left(\boldsymbol{h}_{\bar{n},u,l}^H \mathbf{R}_{c,\bar{n},u,l} \boldsymbol{h}_{\bar{n},u,l}\right)^{-1/2} \mathbf{R}_{c,\bar{n},u,l} \boldsymbol{h}_{\bar{n},u,l}, \tag{33}$$

$$\hat{\mathbf{W}}_{s,\bar{n},l} \hat{\mathbf{W}}_{s,\bar{n},l}^H = \mathbf{R}_{\bar{n}\bar{n},l} - \hat{\mathbf{W}}_{c,\bar{n},l} \hat{\mathbf{W}}_{c,\bar{n},l}^H, \tag{34}$$

constitute the optimal solution to (14) under the orthogonal signal model (30).

Proof. Since the l^{th} OFDM subcarrier is served only by the ISAC node $\bar{n}$, the constraints (32c)–(32e) are exclusively applied to ISAC node $\bar{n}$ for a given l. Provided that $[\mathbf{R}_{\bar{n}\bar{n},l}]_{m,m} = \rho_{\bar{n},m,l} P_T$, where $\sum_{l=1}^{L} \rho_{\bar{n},m,l} \leq 1$, the optimal solution of ($\mathcal{P}$.2) for each l corresponds to that of a single-node ISAC transmit signal design. In other words, the FIM depends only on the diagonal blocks denoted as $\mathbf{R}_{\bar{n}\bar{n},l}$, and the SDP in (32) aligns with a per-node structure for which an optimal rank-one per-user solution can be constructed for the original problem (23) under orthogonal signaling. The remainder of the proof follows the same as in Appendix A of [48]. ∎

Therefore, the orthogonal signal transmission in D-ISAC, utilizing interleaved subcarriers, not only enables efficient D-ISAC transmit signal design but also ensures a rank-one optimal solution from the relaxed optimization problem.

D. Beamforming Design ($\mathcal{P}$.3)

In this section, we focus on a simplified D-ISAC transmit signal design approach based on radar beamforming, diverging from the per-subcarrier signal design strategies discussed in Sections IV-B and IV-C. Instead of optimizing the radar waveform on a per-subcarrier basis, the beamforming design employs a unified spatial precoding structure for sensing signals across all subcarriers. This approach significantly reduces computational complexity while effectively utilizing the spatial degrees of freedom provided by the ISAC system. By emphasizing beamforming for radar waveforms, this method seeks to achieve a balance between system performance and implementation efficiency in D-ISAC signal design.

For the beamforming design in D-ISAC, we apply a block-level beamforming approach to the radar signal, where the signal model is expressed as

$$\mathbf{x}_{s,n,l} = \mathbf{W}_{s,n} \mathbf{s}_{s,l}, \tag{35}$$

where $\mathbf{W}_{s,n}$ represents the unified beamforming matrix for the radar signal. Compared to the signal model for the unconstrained signal design in (15), the beamforming design imposes the condition $\mathbf{W}_{s,n} = \mathbf{W}_{s,n,1} = \cdots = \mathbf{W}_{s,n,L}$, ensuring the same beamforming weights across all subcarriers.

Additionally, to simplify the design further, we incorporate the orthogonal signal condition given in (30). Then, the D-ISAC signal model for the beamforming design is constructed as:

$$\mathbf{x}_{n,l} = \begin{cases} \mathbf{W}_{c,n,l} \mathbf{s}_{c,l} + \mathbf{W}_{s,n} \mathbf{s}_{s,l}, & \text{if } n = l \pmod{N}, \\ \mathbf{0}_{M_t \times 1}, & \text{otherwise}, \end{cases} \tag{36}$$

which allows us to leverage Proposition 1 to further reduce the design variables. The covariance matrix $\mathbf{R}_{\bar{n}\bar{n},l}$ for the specific ISAC node $\bar{n} = l \pmod{N}$ can then be rewritten as:

$$\mathbf{R}_{\bar{n}\bar{n},l} = \sum_{u=1}^{U} \mathbf{R}_{c,\bar{n},u,l} + \mathbf{R}_{s,\bar{n}}, \tag{37}$$

where $\mathbf{R}_{s,\bar{n}}$ is the covariance matrix of the sensing signal for ISAC node $\bar{n}$.

Remark 3: Notably, we observe that the covariance matrix of the sensing signal is independent of the OFDM subcarriers with the signal model for beamforming design. This insight highlights a performance limit that designing beamforming for the sensing signal alone cannot optimize TOF estimates but contributes solely to AOA estimates for target localization.

Based on this observation, we can simplify the optimization problem by introducing the following averaged covariance matrix over the subcarriers:

$$\bar{\mathbf{R}}_{\bar{n}\bar{n}} = \sum_{l=1}^{L} \sum_{u=1}^{U} \mathbf{R}_{c,\bar{n},u,l} + \frac{L}{N} \mathbf{R}_{s,\bar{n}}, \tag{38}$$

where L is assumed to be a multiple of N. By expressing the FIM as a function of the averaged covariance matrix $\frac{N}{L} \bar{\mathbf{R}}_{\bar{n}\bar{n}}$, the transmit signal design contributes solely to AOA measurements in the target localization CRB. Although this relaxation does not provide the optimal solution for the D-ISAC transmit signal design, it reduces computational complexity by

L/N times compared to per-subcarrier sensing signal design approaches, which further will be discussed in Section IV-E.

Consequently, we ignore the dependency on the subcarrier for the target localization FIM $\mathbf{F}$, leading to the relaxed optimization problem for the beamforming design as:

$$(\mathcal{P}.3)\ \underset{\{\mathbf{R}_{c,\bar{n},u,l}\},\{\bar{\mathbf{R}}_{\bar{n}\bar{n}}\}}{\text{minimize}} \quad \sum_{i=1}^{2K} t_i \tag{39a}$$

$$\text{subject to} \quad \text{(23b) and (23c)} \tag{39b}$$

$$\mathbf{R}_{c,\bar{n},u,l} \succeq 0,\ \forall \bar{n}, u, l, \tag{39c}$$

$$\bar{\mathbf{R}}_{\bar{n}\bar{n}} - \sum_{l=1}^{L}\sum_{u=1}^{U} \mathbf{R}_{c,\bar{n},u,l} \succeq 0,\ \forall \bar{n}, \tag{39d}$$

$$\left(1+\frac{1}{\Gamma_c}\right)\mathbf{h}_{\bar{n},u,l}^H \mathbf{R}_{c,\bar{n},u,l}\mathbf{h}_{\bar{n},u,l} - \mathbf{h}_{\bar{n},u,l}^H \mathbf{U}_{\bar{n}\bar{n},l}\mathbf{h}_{\bar{n},u,l} \geq \frac{\sigma_c^2}{L}, \tag{39e}$$

$$\mathbf{U}_{\bar{n}\bar{n},l} = \frac{N}{L}\left(\bar{\mathbf{R}}_{\bar{n}\bar{n}} - \sum_{l=1}^{L}\sum_{u=1}^{U}\mathbf{R}_{c,\bar{n},u,l}\right) + \sum_{u=1}^{U}\mathbf{R}_{c,\bar{n},u,l}. \tag{39f}$$

Although the FIM is evaluated using the averaged covariance matrix $\bar{\mathbf{R}}_{\bar{n}\bar{n}}$, the per-subcarrier communication SINR constraint must still be preserved to ensure communication performance. Thus, the communication SINR constraint (32e) in ($\mathcal{P}.2$) is equivalently expressed as (39e) and (39f) using the variables $\mathbf{R}_{c,\bar{n},u,l}$ and $\bar{\mathbf{R}}_{\bar{n}\bar{n}}$. The formulated problem ($\mathcal{P}.3$) is a standard SDP problem, which can be efficiently solved using a CVX solver.

After solving the convex problem, we obtain $\hat{\mathbf{w}}_{c,\bar{n},u,l}$ using (33). Additionally, the extraction of $\hat{\mathbf{W}}_{s,\bar{n}}$ is revised as:

$$\hat{\mathbf{W}}_{s,\bar{n}}\hat{\mathbf{W}}_{s,\bar{n}}^H = \frac{N}{L}\left(\bar{\mathbf{R}}_{\bar{n}\bar{n}} - \sum_{l=1}^{L}\sum_{u=1}^{U}\mathbf{R}_{c,\bar{n},u,l}\right). \tag{40}$$

Referring to Theorem 2, the relaxation of the rank-one constraint from (23) to ($\mathcal{P}.3$) is tight for the orthogonal signal model as defined in (36). However, it is important to note that the proposed beamforming design in D-ISAC represents a suboptimal solution to (14) because it solely optimizes the signaling for AOA measurements in target localization, without addressing TOF estimation. Nevertheless, it should be noted that the beamforming design is less affected by the increased range sidelobes that may arise in the unconstrained and orthogonal designs. This is because the localization CRB-based signaling design does not capture the impact of range sidelobes introduced by non-uniform subcarrier power allocation. By relying solely on spatial precoding, the beamforming design inherently avoids such subcarrier-domain effects and can thus provide more favorable sidelobe behavior, even though it exhibits inferior CRB performance compared to the other designs.

E. Computational Complexity Analysis

Aligned with the discussions of the three presented D-ISAC signal design approaches, we compare the computational complexity of solving the three different SDP problems: ($\mathcal{P}.1$), ($\mathcal{P}.2$), and ($\mathcal{P}.3$). The time complexity of solving a general SDP problem with variable size $n \times n$ and m constraints using an interior-point algorithm is given as [53]:

$$C_T = O(\sqrt{n}(mn^2 + m^r + n^r)\log(1/\epsilon)), \tag{41}$$

where r is the matrix multiplication exponent and ϵ is the relative accuracy. Accordingly, the complexity is a polynomial function of the number of variables in the specific SDP problem.

Table II
SUMMARY OF D-ISAC TRANSMIT SIGNALING DESIGNS

	D-ISAC Signal Model	Signal Correlation	Number of Variables
Unconstrained ($\mathcal{P}.1$)	$\mathbf{W}_{c,n,l}\mathbf{s}_{c,l} + \mathbf{W}_{s,n,l}\mathbf{s}_{s,l}$	Non-orthogonal	$M_t^2N^2L + M_t^2NUL$
Orthogonal ($\mathcal{P}.2$)	$\mathbf{W}_{c,n,l}\mathbf{s}_{c,l} + \mathbf{W}_{s,n,l}\mathbf{s}_{s,l}$	Orthogonal	$M_t^2(L{+}UL)$
Beamforming ($\mathcal{P}.3$)	$\mathbf{W}_{c,n,l}\mathbf{s}_{c,l} + \mathbf{W}_{s,n}\mathbf{s}_{s,l}$	Orthogonal	$M_t^2(N + UL)$

Let us denote Q_1, Q_2, and Q_3 as the total number of variables for each problem ($\mathcal{P}.1$), ($\mathcal{P}.2$), and ($\mathcal{P}.3$), respectively, which are computed as

$$Q_1 = M_t^2N^2L + M_t^2NUL, \tag{42}$$

$$Q_2 = M_t^2(L + UL), \tag{43}$$

$$Q_3 = M_t^2(N + UL). \tag{44}$$

Compared to the unconstrained signal design problem ($\mathcal{P}.1$), the orthogonal signal transmission results in significantly lower complexity in ($\mathcal{P}.2$), as these approaches do not consider signal cross-correlations between different nodes. The complexity of ($\mathcal{P}.1$) increases substantially with the number of subcarriers L. Furthermore, given that $L \gg N$ where the number of subcarriers is much larger than the number of cooperative ISAC nodes, the beamforming design ($\mathcal{P}.3$) exhibits even lower complexity since it focuses solely on optimizing AOA measurements for target localization and does not require subcarrier-by-subcarrier signal design. The summary of three different types of designs is provided in Table II.

V. NUMERICAL SIMULATION RESULTS

In this section, we present numerical simulation results for the proposed D-ISAC transmit signal design methods. The results focus on the performance trade-off between sensing and communication in the D-ISAC system using the proposed transmit signal designs. Additionally, we investigate the effects of various system parameters to provide insights into the TOF-AOA hybrid localization method and the three different types of D-ISAC signal designs. Unless stated otherwise, the default system parameters are set as follows: $P_T/\sigma_c^2 = P_T/\sigma_s^2 = 20$ dB, the number of transmit and receive antennas per ISAC node $M = M_t = M_r = 6$, and the number of OFDM subcarriers $L = 16$. The communication channel is modeled as a Rayleigh fading channel, with normalized channel gain to simplify the analysis for the multi-user scenario. The average target amplitude $\sum_{k=1}^{K}\sum_{n=1}^{N}\sum_{m=1}^{N}|b_{n,m}^k|^2/KN^2$ is fixed to 10 dB.

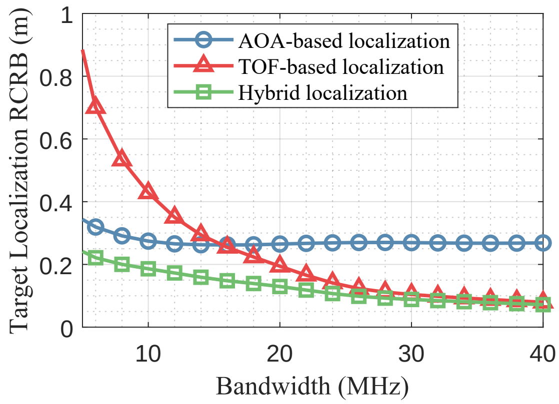

(a)

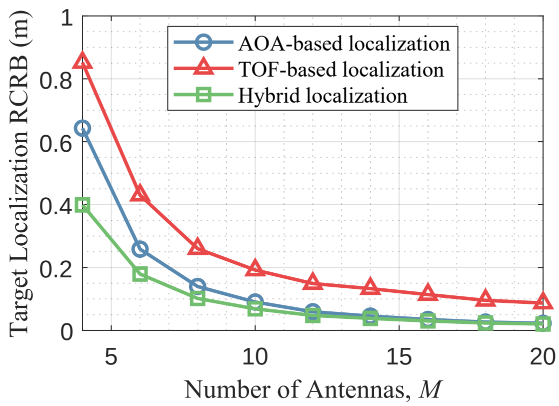

(b)

Fig. 4. Performance comparisons between AOA-based, TOF-based, and hybrid localization methods under varying D-ISAC system parameters: target localization RCRB vs. (a) signal bandwidth with $M = 6$, and (b) the number of antennas, keeping the total power constant, with a 10-MHz signal bandwidth. The designed D-ISAC signal with $\Gamma_c = 30$ dB is used for evaluation with $K = 2, U = 2$.

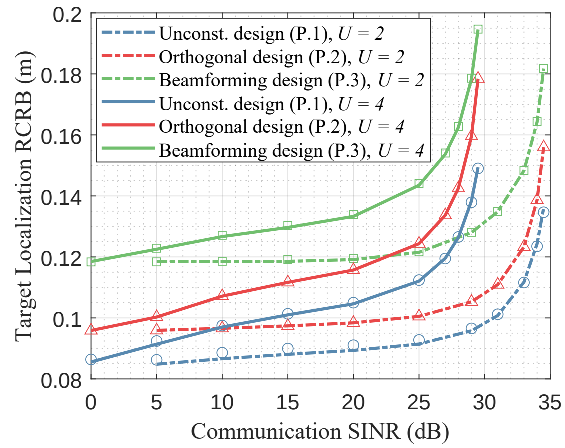

Fig. 5. ISAC trade-off performances of the proposed D-ISAC transmit signal designs with varying numbers of users. The number of targets is $K = 2$. The markers (○, △, and □) on the lines represent the extracted solutions derived from the optimal solutions of the respective SDP problems.

A. Comparisons of Target Localization Methods

We first examine the target localization methods for D-ISAC. The proposed D-ISAC system utilizes a hybrid TOF and AOA localization approach, leveraging all possible measurements to localize targets. This method combines the advantages of both collocated MIMO and distributed MIMO radar sensing. For this simulation, four ISAC nodes ($N = 4$) are positioned at $[-46.19\,\text{m}, -19.13\,\text{m}]$, $[46.19\,\text{m}, -19.13\,\text{m}]$, $[-19.13\,\text{m}, -46.19\,\text{m}]$, and $[19.13\,\text{m}, -46.19\,\text{m}]$ with their antenna arrays oriented toward the origin. This corresponds to a 50 m distance from each node to the origin. Two users are located at $[0\,\text{m}, -20\,\text{m}]$ and $[0\,\text{m}, 20\,\text{m}]$, and two targets are positioned at $[0\,\text{m}, 0\,\text{m}]$ and $[0\,\text{m}, 10\,\text{m}]$, respectively. To compare the target localization performance depending on localization methods, we employed the D-ISAC signaling with the orthogonal design ($\mathcal{P}.2$). This choice was made because the sensing performance trends remain consistent across all signaling designs for the different localization methods. The CRB for the TOF-based localization method is evaluated by setting $\dot{\mathbf{A}}_{r,n}$ and $\dot{\mathbf{A}}_{t,n}$ to zero, while the CRB for the AOA-based localization method is evaluated by setting $\dot{\mathbf{D}}_n$ to zero in the FIM.

The results in Fig. 4 demonstrate the superior localization root-CRB (RCRB) of the hybrid localization method compared to the other two approaches. However, the performance trends among these methods vary depending on the system parameters. For instance, increasing the signal bandwidth primarily improves TOF measurements, as shown in Fig. 4(a). This validates that the performance of the TOF-based localization method converges toward that of the hybrid approach with wideband D-ISAC systems. Conversely, increasing the number of antennas in the D-ISAC system significantly enhances the AOA-based localization performance compared to the TOF-based method in Fig. 4(b). This is because the TOF-based localization benefits only from increased SNR owing to beamforming gain, whereas the AOA-based method further exploits the advantages of the larger array aperture size. These observations are closely linked to the ISAC performance comparisons among the proposed three different types of transmit signal designs, which will be further discussed in the following section.

B. ISAC Performance of D-ISAC Signaling Designs

In this section, we evaluate the ISAC trade-off performances among three different D-ISAC designs: unconstrained signal design ($\mathcal{P}.1$), orthogonal design ($\mathcal{P}.2$), and beamforming design ($\mathcal{P}.3$). For the simulation setup, we consider multi-target and multi-user scenarios. Radar targets are positioned linearly along the x-axis between $-30\,\text{m}$ and $30\,\text{m}$, with $y_k = 0, \forall k \in \{1, \ldots, K\}$. Similarly, communication users are positioned linearly along the y-axis between $-20\,\text{m}$ and $20\,\text{m}$, with $x_u = 0, \forall u \in \{1, \ldots, U\}$. The number of ISAC nodes is $N = 2$, consistent with Section V-A, and the OFDM signal bandwidth is set to $20\,\text{MHz}$.

First, we validate the CRB-SINR trade-offs of the three designs, as shown in Fig. 5 and Fig. 6. The proposed D-ISAC transmit signal designs clearly demonstrate trade-offs between sensing and communication performance. As expected, the unconstrained signal design ($\mathcal{P}.1$) achieves the best sensing performance compared to the other two designs utilizing orthogonal signal transmission. This result indicates

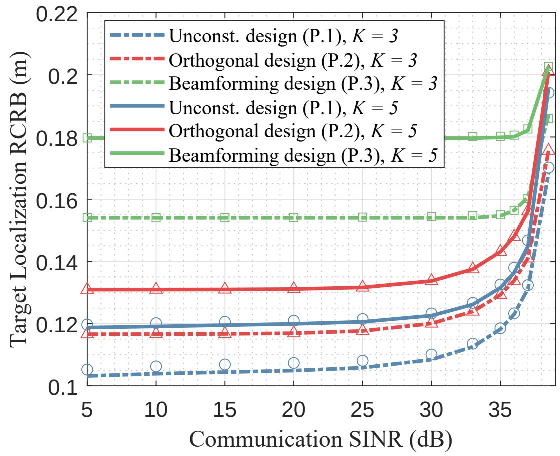

Fig. 6. ISAC trade-off performances of the proposed D-ISAC transmit signal designs with varying numbers of targets. The number of users is $U = 1$. The markers (○, △, and □) on the lines represent the extracted solutions derived from the optimal solutions of the respective SDP problems.

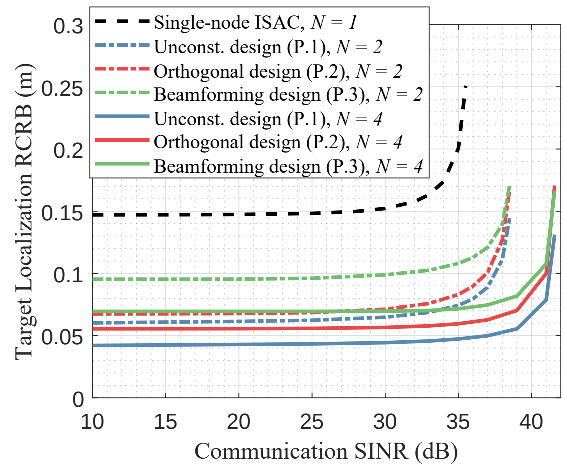

Fig. 7. ISAC trade-off performances of the proposed D-ISAC transmit signal designs with varying numbers of ISAC nodes. The number of targets and users is $K = 1, U = 1$. Each node is equipped with $M = 6$.

that orthogonal signals for distributed MIMO radar do not guarantee optimal sensing performance for target localization.

Furthermore, the overall ISAC performance degrades as the number of users increases in all three designs, and the maximum achievable communication SINR also decreases, as shown in Fig. 5. Conversely, an increase in the number of targets degrades the target localization RCRB, while the maximum achievable communication SINR remains unchanged, as shown in Fig. 6. Interestingly, the performance gap trends between the three designs remain consistent regardless of the number of users or targets. This observation implies that the differences between the designs lie solely in the signal modeling and do not affect the degree-of-freedom (DoF) of the transmitter design.

As discussed in Theorem 2, the optimal solution of the relaxed problem with the orthogonal signal model is also the optimal solution of the original problem without the rank-one constraint relaxation. This is validated by the markers on the lines in each plot, which indicate the performance of the extracted solutions derived from the relaxed problem's solutions. Notably, the extracted solution of ($\mathcal{P}.1$), which serves as an approximate solution, does not deviate significantly from the convex optimization bound. However, it exhibits degraded performance when the communication SINR is set to relatively low values. This degradation arises because the rank of $\widehat{\widetilde{\mathbf{R}}}_{s,l}$ in (28) may become deficient due to the approximation to a positive semidefinite matrix.

In Fig. 7, we illustrate the ISAC performance gain of D-ISAC with varying numbers of cooperative nodes. For the case of $N = 4$, the ISAC nodes are positioned at $[-46.19\,\text{m}, -19.13\,\text{m}]$, $[46.19\,\text{m}, -19.13\,\text{m}]$, $[-19.13\,\text{m}, -46.19\,\text{m}]$, and $[19.13\,\text{m}, -46.19\,\text{m}]$, all equidistant from the origin. As the number of cooperative nodes increases, we observe performance improvements in both sensing and communication. From the perspective of communication performance, this cooperation gain stems from noncoherent CoMP transmission, which leverages the power combining gain of distributed ISAC nodes. For target localization, the performance gain arises from the noncoherent processing of the distributed MIMO radar, utilizing TOF measurements to localize the target [33]. It is worth noting that the cooperative sensing gain is significantly influenced by the geometric relationship between target and node positions [44]. Moreover, the optimal number of distributed ISAC nodes can be determined by considering antenna-to-node allocation under a given cooperative node density [19]. For a more detailed analysis of target localization performance in noncoherent distributed sensing with randomly deployed ISAC nodes, we refer readers to [19].

Furthermore, the performance gain of noncoherent D-ISAC is fundamentally constrained by the level of time–frequency synchronization achievable in practice. In particular, time offsets between ISAC nodes introduce biased TOF measurements in bi-static links, which directly degrade the target localization accuracy in distributed ISAC systems [54], [55]. Achieving precise synchronization across physically separated nodes therefore remains a critical bottleneck for fully realizing the cooperative sensing gains of networked ISAC. This underscores the importance of developing advanced over-the-air time–frequency synchronization techniques that are robust to complex propagation environments and practical hardware impairments, thereby enabling reliable and scalable noncoherent D-ISAC operation.

C. Effects of System Parameters

We explore the effects of D-ISAC system parameters on the performance of the proposed transmit signal designs. Here, we showcase the performance variations with respect to the signal bandwidth and the number of antennas. In Fig. 8, the target localization CRBs as a function of the signal bandwidth are depicted. Interestingly, the performance of the orthogonal design ($\mathcal{P}.2$) converges to that of the unconstrained design ($\mathcal{P}.1$) as the signal bandwidth increases. This phenomenon can be explained as follows: TOF measurements predominantly contribute to target localization performance in wideband systems, as discussed in Section V-A. Since both ($\mathcal{P}.1$) and

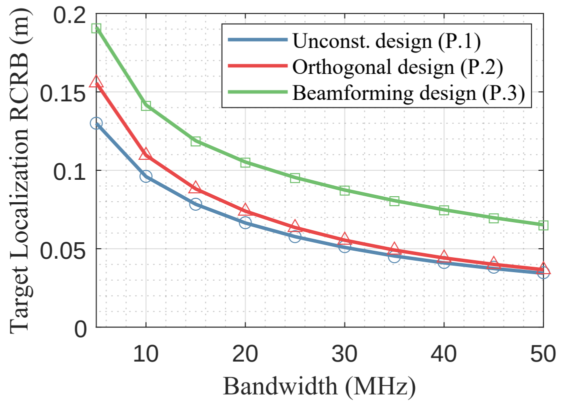

Fig. 8. Performance comparisons of three different designs ($\mathcal{P}.1$), ($\mathcal{P}.2$), and ($\mathcal{P}.3$) with $U = 1$, $K = 1$, and $\Gamma_c = 30$ dB under varying signal bandwidth with $M = 6$.

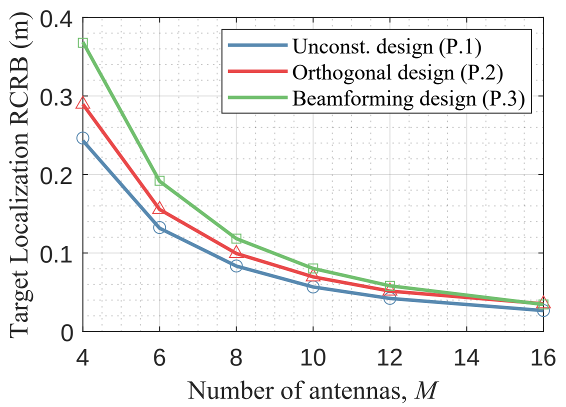

Fig. 9. Performance comparisons of three different designs ($\mathcal{P}.1$), ($\mathcal{P}.2$), and ($\mathcal{P}.3$) with $U = 1$, $K = 1$, and $\Gamma_c = 30$ dB under varying numbers of antennas, keeping the total power constant, with a 5-MHz signal bandwidth.

($\mathcal{P}.2$) employ per-subcarrier signal designs optimized for TOF estimation, their performances become similar with increasing signal bandwidth. The primary difference between the two lies in the consideration of signal cross-correlation between ISAC nodes, which is more relevant to AOA estimation performance.

Conversely, as the number of antennas increases, the performance of the orthogonal design ($\mathcal{P}.2$) converges to that of the beamforming design ($\mathcal{P}.3$). Unlike the case of increasing signal bandwidth, a larger number of antennas enhances AOA estimation performance, and the hybrid localization performance becomes dominated by AOA measurements. Consequently, the per-subcarrier signal designs in ($\mathcal{P}.1$) and ($\mathcal{P}.2$) become less effective when AOA measurements predominantly determine target localization performance.

D. Computational Complexity

Followed by the computational complexity analysis in Section IV-E, we empirically evaluate the execution time of each D-ISAC transmit signal design. The measured execution times are averaged over 100 trials. For all three design methods, the execution time increases with the number of subcarriers, consistent with the complexity trends discussed in (42)–(44). As expected, the unconstrained signal design ($\mathcal{P}.1$) exhibits the longest execution time among the three designs. Combined with the ISAC performances described in Section V-B, the three designs demonstrate clear performance-complexity trade-offs. Consequently, one can select an appropriate design based on the system requirements such as computational resources.

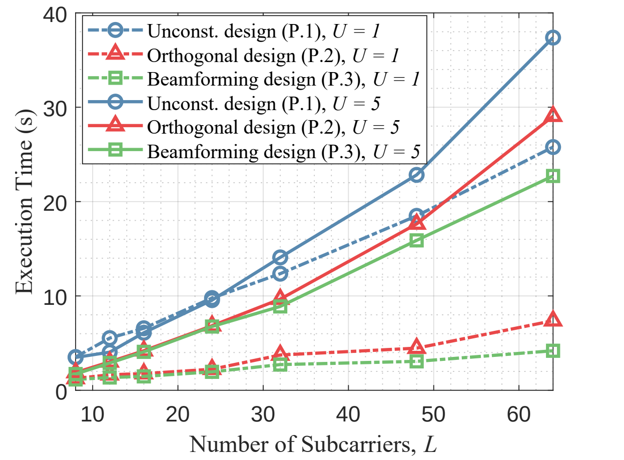

Fig. 10. Comparisons of the execution time with respect to the number of subcarriers with $K = 1$.

Table III
COMPARISONS OF THE EXECUTION TIME WITH RESPECT TO THE NUMBER OF NODES WITH $K = 1$ AND $U = 1$

	$N = 2$	$N = 3$	$N = 4$
Unconstrained design (P.1)	2.92 s	7.66 s	52.86 s
Orthogonal design (P.2)	1.78 s	2.96 s	12.7 s
Beamforming design (P.3)	1.16 s	1.45 s	8.82 s

As demonstrated, the proposed SDR-based solutions exhibit relatively long running times due to the large number of optimization variables in MIMO–OFDM D-ISAC. This issue is common in MIMO–OFDM precoding designs, where precoders must be optimized for every subcarrier under frequency-selective fading channels [56], [57]. To alleviate this high complexity, several approaches can be adopted, such as interpolation-based methods [58] and subcarrier clustering techniques [59]. Moreover, further reductions in complexity can be achieved by developing efficient solvers such as successive convex approximation (SCA) and alternating optimization, which represent promising directions for future research.

E. Discussions

The proposed framework for MIMO–OFDM signaling design in D-ISAC adopts the deterministic CRB of target localization as the sensing performance metric and assumes full CSI knowledge except for phase coherency across nodes. This setting establishes the fundamental sensing–communication trade-off performance for noncoherent D-ISAC systems. In practice, however, the Bayesian CRB, which incorporates prior knowledge of target parameters, together with limited CSI conditions, may offer a more practical formulation for realworld scenarios [60], [61]. Therefore, extending the proposed framework to incorporate Bayesian CRB and imperfect CSI assumptions represents a promising direction to further enhance the applicability of distributed ISAC signaling design.

Moreover, in the context of distributed configurations, the use of reconfigurable intelligent surfaces (RIS) has the potential to reduce implementation cost while enabling large-scale cooperative sensing and communication [62], [63]. Accordingly, investigating transmit signaling design in RIS-assisted D-ISAC systems could open up new opportunities for developing cost-effective and scalable solutions to support distributed sensing and communication on an unprecedented scale.

VI. Conclusions

This work presents a D-ISAC transmit signal design framework that enhances radar and communication functionalities through the cooperation of distributed ISAC systems. By leveraging both collocated and distributed MIMO radar, the proposed framework integrates AOA and TOF measurements for precise target localization, while improving communication SINR via the power combining gain of CoMP transmission. CRB-SINR-based optimization problems are formulated, and three different transmit signal designs, unconstrained, orthogonal, and beamforming, are introduced, highlighting trade-offs between ISAC performance and computational complexity. Numerical simulations validate the effectiveness of the proposed designs, providing insights into D-ISAC performance bounds, system parameter impacts, and performance-complexity trade-offs. These findings emphasize the importance of advanced transmit signal designs in unlocking the full potential of D-ISAC systems for future wireless networks. Future work will explore system-level aspects such as time-frequency synchronization, phase coherency, and efficient D-ISAC receiver processing and fusion, which may significantly influence overall D-ISAC performance.

Appendix A
Derivation of the FIM for D-ISAC target localization

The Jacobian matrix for the target localization is derived as

$$\mathbf{J} = \begin{bmatrix} \frac{\partial \boldsymbol{\theta}}{\partial \mathbf{x}} & \frac{\partial \boldsymbol{\tau}}{\partial \mathbf{x}} & \mathbf{0} & \mathbf{0} \\ \frac{\partial \boldsymbol{\theta}}{\partial \mathbf{y}} & \frac{\partial \boldsymbol{\tau}}{\partial \mathbf{y}} & \mathbf{0} & \mathbf{0} \\ \mathbf{0} & \mathbf{0} & \mathbf{I}_{KN^2} & \mathbf{0} \\ \mathbf{0} & \mathbf{0} & \mathbf{0} & \mathbf{I}_{KN^2} \end{bmatrix}. \tag{45}$$

Each entry of the partial derivatives $\frac{\partial \boldsymbol{\theta}}{\partial \mathbf{x}}$, $\frac{\partial \boldsymbol{\theta}}{\partial \mathbf{y}}$, $\frac{\partial \boldsymbol{\tau}}{\partial \mathbf{x}}$, and $\frac{\partial \boldsymbol{\tau}}{\partial \mathbf{y}} \in \mathbb{R}^{K \times NK}$ is respectively obtained as $\frac{\partial \theta_n^k}{\partial x_k} = \frac{y_n - y_k}{(x_k - x_n)^2 + (y_k - y_n)^2}$, $\frac{\partial \theta_n^k}{\partial y_k} = \frac{x_k - x_n}{(x_k - x_n)^2 + (y_k - y_n)^2}$, $\frac{\partial \tau_n^k}{\partial x_k} = \frac{x_k - x_n}{c\sqrt{(x_k - x_n)^2 + (y_k - y_n)^2}}$, and $\frac{\partial \tau_n^k}{\partial y_k} = \frac{y_k - y_n}{c\sqrt{(x_k - x_n)^2 + (y_k - y_n)^2}}$.

Then, we derive the FIM $\mathbf{F}(\boldsymbol{\Psi})$ for noncoherent D-ISAC systems. For simplicity of the derivation, $\mathbf{F}(\boldsymbol{\Psi})$ can be expressed as a following block matrix:

$$\mathbf{F}(\boldsymbol{\Psi}) = \frac{2}{\sigma^2} \mathrm{Re}\left\{ \mathbb{E}\left(\begin{bmatrix} \mathbf{T} & \mathbf{E} \\ \mathbf{E}^T & \mathbf{G} \end{bmatrix} \right) \right\}, \tag{46}$$

where $\mathbf{T} \in \mathbb{C}^{2KN \times 2KN}$, $\mathbf{E} \in \mathbb{C}^{2KN \times 2KN^2}$, and $\mathbf{G} \in \mathbb{C}^{2KN^2 \times 2KN^2}$. First, the submatrix $\mathbf{T}$ is also represented as

$$\mathbf{T} = \begin{bmatrix} \mathbf{F}_{\boldsymbol{\theta\theta}} & \mathbf{F}_{\boldsymbol{\theta\tau}} \\ \mathbf{F}_{\boldsymbol{\theta\tau}}^T & \mathbf{F}_{\boldsymbol{\tau\tau}} \end{bmatrix}. \tag{47}$$

We redefine parameters of interest as $\boldsymbol{\theta} = [\boldsymbol{\theta}_1^T, \boldsymbol{\theta}_2^T, \ldots, \boldsymbol{\theta}_N^T]^T$ and $\boldsymbol{\tau} = [\boldsymbol{\tau}_1^T, \boldsymbol{\tau}_2^T, \ldots, \boldsymbol{\tau}_N^T]^T$, where $\boldsymbol{\theta}_n = [\theta_n^1, \theta_n^2, \ldots, \theta_n^k]^T$ and $\boldsymbol{\tau}_n = [\tau_n^1, \tau_n^2, \ldots, \tau_n^k]^T$ for $n = 1, 2, ..., N$. Also, $\mathbf{F}_{\boldsymbol{\theta\theta}}, \mathbf{F}_{\boldsymbol{\theta\tau}}$, and $\mathbf{F}_{\boldsymbol{\tau\tau}}$ are again partitioned into the block matrix with $K \times K$ submatrices denoted as $\mathbf{F}_{\boldsymbol{\theta}_n\boldsymbol{\theta}_m}, \mathbf{F}_{\boldsymbol{\theta}_n\boldsymbol{\tau}_m}$, and $\mathbf{F}_{\boldsymbol{\tau}_n\boldsymbol{\tau}_m}$ for $n = 1, 2, ..., N$ and $m = 1, 2, ..., N$. Then, each submatrix in (47) can be developed as

$$\begin{aligned}
\left\{\mathbf{F}_{\boldsymbol{\theta}_n\boldsymbol{\theta}_m}\right\}_{n=m} &= (\dot{\mathbf{A}}_{r,n}^H \dot{\mathbf{A}}_{r,n}) \odot (\mathbf{P}_n^H \mathbf{P}_n) \\
&\quad + (\dot{\mathbf{A}}_{r,n}^H \mathbf{A}_{r,n}) \odot (\mathbf{P}_n^H \dot{\mathbf{V}}_{\theta_n,n,n} \mathbf{B}_{n,n}) \\
&\quad + (\mathbf{A}_{r,n}^H \dot{\mathbf{A}}_{r,n}) \odot (\mathbf{B}_{n,n}^* \dot{\mathbf{V}}_{\theta_n,n,n}^H \mathbf{P}_n) \\
&\quad + \sum_{i=1}^{N} (\mathbf{A}_{r,i}^H \mathbf{A}_{r,i}) \odot (\mathbf{B}_{i,n}^* \dot{\mathbf{V}}_{\theta_n,i,n}^H \dot{\mathbf{V}}_{\theta_n,i,n} \mathbf{B}_{i,n}), \quad (48a)\\
\left\{\mathbf{F}_{\boldsymbol{\theta}_n\boldsymbol{\theta}_m}\right\}_{n\neq m} &= (\dot{\mathbf{A}}_{r,n}^H \mathbf{A}_{r,n}) \odot (\mathbf{P}_n^H \dot{\mathbf{V}}_{\theta_m,n,m} \mathbf{B}_{n,m}) \\
&\quad + (\mathbf{A}_{r,m}^H \dot{\mathbf{A}}_{r,m}) \odot (\mathbf{B}_{m,n}^* \dot{\mathbf{V}}_{\theta_n,m,n}^H \mathbf{P}_m) \\
&\quad + \sum_{i=1}^{N} (\mathbf{A}_{r,i}^H \mathbf{A}_{r,i}) \odot (\mathbf{B}_{i,n}^* \dot{\mathbf{V}}_{\theta_n,i,n}^H \dot{\mathbf{V}}_{\theta_m,i,m} \mathbf{B}_{i,m}), \quad (48b)\\
\left\{\mathbf{F}_{\boldsymbol{\theta}_n\boldsymbol{\tau}_m}\right\}_{n=m} &= (\dot{\mathbf{A}}_{r,n}^H \mathbf{A}_{r,n}) \odot (\mathbf{P}_n^H \dot{\mathbf{P}}_{\tau_n,n}) \\
&\quad + (\dot{\mathbf{A}}_{r,n}^H \mathbf{A}_{r,n}) \odot (\mathbf{P}_n^H \dot{\mathbf{V}}_{\tau_n,n,n} \mathbf{B}_{n,n}) \\
&\quad + (\mathbf{A}_{r,n}^H \mathbf{A}_{r,n}) \odot (\mathbf{B}_{n,n}^* \dot{\mathbf{V}}_{\theta_n,n,n}^H \dot{\mathbf{P}}_{\tau_n,n}) \\
&\quad + \sum_{i=1}^{N} (\mathbf{A}_{r,i}^H \mathbf{A}_{r,i}) \odot (\mathbf{B}_{i,n}^* \dot{\mathbf{V}}_{\theta_n,i,n}^H \dot{\mathbf{V}}_{\tau_n,i,n} \mathbf{B}_{i,n}), \quad (48c)\\
\left\{\mathbf{F}_{\boldsymbol{\theta}_n\boldsymbol{\tau}_m}\right\}_{n\neq m} &= (\dot{\mathbf{A}}_{r,n}^H \mathbf{A}_{r,n}) \odot (\mathbf{P}_n^H \dot{\mathbf{V}}_{\tau_m,n,m} \mathbf{B}_{n,m}) \\
&\quad + (\mathbf{A}_{r,m}^H \mathbf{A}_{r,m}) \odot (\mathbf{B}_{m,n}^* \dot{\mathbf{V}}_{\theta_n,m,n}^H \dot{\mathbf{P}}_{\tau_m,m}) \\
&\quad + \sum_{i=1}^{N} (\mathbf{A}_{r,i}^H \mathbf{A}_{r,i}) \odot (\mathbf{B}_{i,n}^* \dot{\mathbf{V}}_{\theta_n,i,n}^H \dot{\mathbf{V}}_{\tau_m,i,m} \mathbf{B}_{i,m}), \quad (48d)\\
\left\{\mathbf{F}_{\boldsymbol{\tau}_n\boldsymbol{\tau}_m}\right\}_{n=m} &= (\mathbf{A}_{r,n}^H \mathbf{A}_{r,n}) \odot (\dot{\mathbf{P}}_{\tau_n,n}^H \dot{\mathbf{P}}_{\tau_n,n}) \\
&\quad + (\mathbf{A}_{r,n}^H \mathbf{A}_{r,n}) \odot (\dot{\mathbf{P}}_{\tau_n,n}^H \dot{\mathbf{V}}_{\tau_n,n,n} \mathbf{B}_{n,n}) \\
&\quad + (\mathbf{A}_{r,n}^H \mathbf{A}_{r,n}) \odot (\mathbf{B}_{n,n}^* \dot{\mathbf{V}}_{\tau_n,n,n}^H \dot{\mathbf{P}}_{\tau_n,n}) \\
&\quad + \sum_{i=1}^{N} (\mathbf{A}_{r,i}^H \mathbf{A}_{r,i}) \odot (\mathbf{B}_{i,n}^* \dot{\mathbf{V}}_{\tau_n,i,n}^H \dot{\mathbf{V}}_{\tau_n,i,n} \mathbf{B}_{i,n}), \quad (48e)\\
\left\{\mathbf{F}_{\boldsymbol{\tau}_n\boldsymbol{\tau}_m}\right\}_{n\neq m} &= (\mathbf{A}_{r,n}^H \mathbf{A}_{r,n}) \odot (\dot{\mathbf{P}}_{\tau_n,n}^H \dot{\mathbf{V}}_{\tau_m,n,m} \mathbf{B}_{n,m}) \\
&\quad + (\mathbf{A}_{r,m}^H \mathbf{A}_{r,m}) \odot (\mathbf{B}_{m,n}^* \dot{\mathbf{V}}_{\tau_n,m,n}^H \dot{\mathbf{P}}_{\tau_m,m}) \\
&\quad + \sum_{i=1}^{N} (\mathbf{A}_{r,i}^H \mathbf{A}_{r,i}) \odot (\mathbf{B}_{i,n}^* \dot{\mathbf{V}}_{\tau_n,i,n}^H \dot{\mathbf{V}}_{\tau_m,i,m} \mathbf{B}_{i,m}), \quad (48f)
\end{aligned}$$

where $\mathbf{F}_{\boldsymbol{\theta}_n\boldsymbol{\theta}_m}$ is the (m, n) submatrix of $\mathbf{F}_{\boldsymbol{\theta\theta}}$. All derivatives with respect to unknown variables and related expressions are defined as $\mathbf{P}_n = \sum_{m=1}^{N} \left(\mathbf{B}_{n,m} \mathbf{V}_{n,m}^T\right)^T$, $\dot{\mathbf{P}}_{\tau_n,n} = \sum_{m=1}^{N} \left(\mathbf{B}_{n,m} \dot{\mathbf{V}}_{\tau_n,n,m}^T\right)^T$, $\dot{\mathbf{V}}_{\theta_m,n,m} = \mathbf{X}_m^T \dot{\mathbf{A}}_{t,m} \odot \mathbf{D}_{n,m}$, $\dot{\mathbf{V}}_{\tau_n,n,m} = \dot{\mathbf{V}}_{\tau_m,n,m} = \mathbf{X}_m^T \mathbf{A}_{t,m} \odot \dot{\mathbf{D}}_{n,m}$.

Similar to (47), $\mathbf{E}$ and $\mathbf{G}$ also can be represented as $\mathbf{E} = \begin{bmatrix} \mathbf{F}_{\boldsymbol{\theta}\mathbf{b}} & j\mathbf{F}_{\boldsymbol{\theta}\mathbf{b}} \\ \mathbf{F}_{\boldsymbol{\tau}\mathbf{b}} & j\mathbf{F}_{\boldsymbol{\tau}\mathbf{b}} \end{bmatrix}$, $\mathbf{G} = \begin{bmatrix} \mathbf{F}_{\mathbf{bb}} & j\mathbf{F}_{\mathbf{bb}} \\ j\mathbf{F}_{\mathbf{bb}}^T & \mathbf{F}_{\mathbf{bb}} \end{bmatrix}$. Let us redefine

$\mathbf{b} = [\mathbf{b}_1^T, \mathbf{b}_2^T, \ldots, \mathbf{b}_N^T]^T$, where $\mathbf{b}_n = [\mathbf{b}_{n,1}^T, \mathbf{b}_{n,2}^T, \ldots, \mathbf{b}_{n,N}^T]^T$ and $\mathbf{b}_{n,m} = [b_{n,m}^1, b_{n,m}^2, \ldots, b_{n,m}^K]^T$. By using the same notation with (48), each submatrix in $\mathbf{E}$ is derived as follows: $\mathbf{F}_{\theta_n \mathbf{b}_m} = \left[\mathbf{F}_{\theta_n \mathbf{b}_{m,1}}, \mathbf{F}_{\theta_n \mathbf{b}_{m,2}}, \ldots, \mathbf{F}_{\theta_n \mathbf{b}_{m,N}}\right]$, $\mathbf{F}_{\tau_n \mathbf{b}_m} = \left[\mathbf{F}_{\tau_n \mathbf{b}_{m,1}}, \mathbf{F}_{\tau_n \mathbf{b}_{m,2}}, \ldots, \mathbf{F}_{\tau_n \mathbf{b}_{m,N}}\right]$, where

$$\left\{\mathbf{F}_{\theta_n \mathbf{b}_{m,i}}\right\}_{n=m} = (\dot{\mathbf{A}}_{r,n}^H \mathbf{A}_{r,n}) \odot (\mathbf{P}_n^H \mathbf{V}_{n,i}) + (\mathbf{A}_{r,n}^H \mathbf{A}_{r,n}) \odot (\mathbf{B}_{n,n}^* \dot{\mathbf{V}}_{\theta_n,n,n}^H \mathbf{V}_{n,i}) \tag{49a}$$

$$\left\{\mathbf{F}_{\theta_n \mathbf{b}_{m,i}}\right\}_{n\neq m} = (\mathbf{A}_{r,m}^H \mathbf{A}_{r,m}) \odot (\mathbf{B}_{m,n}^* \dot{\mathbf{V}}_{\theta_n,m,n}^H \mathbf{V}_{m,i}), \tag{49b}$$

$$\left\{\mathbf{F}_{\tau_n \mathbf{b}_{m,i}}\right\}_{n=m} = (\mathbf{A}_{r,n}^H \mathbf{A}_{r,n}) \odot (\dot{\mathbf{P}}_{\tau_n,n}^H \mathbf{V}_{n,i}) + (\mathbf{A}_{r,n}^H \mathbf{A}_{r,n}) \odot (\mathbf{B}_{n,n}^* \dot{\mathbf{V}}_{\tau_n,n,n}^H \mathbf{V}_{n,i}). \tag{49c}$$

$$\left\{\mathbf{F}_{\tau_n \mathbf{b}_{m,i}}\right\}_{n\neq m} = (\mathbf{A}_{r,m}^H \mathbf{A}_{r,m}) \odot (\mathbf{B}_{m,n}^* \dot{\mathbf{V}}_{\tau_n,m,n}^H \mathbf{V}_{m,i}). \tag{49d}$$

Lastly, the submatrix component in $\mathbf{G}$ is written as

$$\mathbf{F}_{\mathbf{bb}} = \operatorname{diag}\left(\mathbf{F}_{\mathbf{b}_1\mathbf{b}_1}, \mathbf{F}_{\mathbf{b}_2\mathbf{b}_2}, \ldots, \mathbf{F}_{\mathbf{b}_N\mathbf{b}_N}\right), \tag{50}$$

where

$$\mathbf{F}_{\mathbf{b}_{n,i}\mathbf{b}_{n,j}} = (\mathbf{A}_{r,n}^H \mathbf{A}_{r,n}) \odot (\mathbf{V}_{n,i}^H \mathbf{V}_{n,j}). \tag{51}$$

Augmenting all blocks into (46) yields the complete FIM for the noncoherent D-ISAC target localization.

Appendix B
Proof of Theorem 2

First, we note that $\mathbf{R}_{nn,l}$ is the diagonal submatrix of $\mathbf{R}_l$, which satisfies the constraint (23b). Therefore, $\tilde{\mathbf{R}}_{nn,l}$ also satisfies (23b). Moreover, it is straightforward to verify that

$$\mathbf{h}_{n,u,l}^H \tilde{\mathbf{R}}_{c,n,u,l} \mathbf{h}_{n,u,l} = \mathbf{h}_{n,u,l}^H \mathbf{R}_{c,n,u,l} \mathbf{h}_{n,u,l}, \tag{52}$$

which proves that the constraint (23f) also holds.

Next, we exploit the fact that $\mathbf{R}_{c,n,u,l} - \tilde{\mathbf{R}}_{c,n,u,l} \succeq 0$ to establish that (24d) holds for $\tilde{\mathbf{R}}_{c,n,u,l}, \forall n,u,l$ [48]. For any $\mathbf{u} \in \mathbb{C}^{M_t \times 1}$, we can write

$$\mathbf{u}^H (\mathbf{R}_{c,n,u,l} - \tilde{\mathbf{R}}_{c,n,u,l}) \mathbf{u} = \mathbf{u}^H \mathbf{R}_{c,n,u,l} \mathbf{u} - \frac{|\mathbf{u}^H \mathbf{R}_{c,n,u,l} \mathbf{h}_{n,u,l}|^2}{\mathbf{h}_{n,u,l}^H \mathbf{R}_{c,n,u,l} \mathbf{h}_{n,u,l}}. \tag{53}$$

By the Cauchy–Schwarz inequality,

$$\left(\mathbf{h}_{n,u,l}^H \mathbf{R}_{c,n,u,l} \mathbf{h}_{n,u,l}\right)\left(\mathbf{u}^H \mathbf{R}_{c,n,u,l} \mathbf{u}\right) \geq \left|\mathbf{u}^H \mathbf{R}_{c,n,u,l} \mathbf{h}_{n,u,l}\right|^2, \tag{54}$$

which implies

$$\mathbf{u}^H (\mathbf{R}_{c,n,u,l} - \tilde{\mathbf{R}}_{c,n,u,l}) \mathbf{u} \geq 0, \tag{55}$$

and thus $\mathbf{R}_{c,n,u,l} - \tilde{\mathbf{R}}_{c,n,u,l} \succeq 0$.

Therefore, constraint (24d) can be rewritten as

$$\tilde{\mathbf{R}}_{nn,l} - \sum_{u=1}^{U} \tilde{\mathbf{R}}_{c,n,u,l} = \mathbf{R}_{nn,l} - \sum_{u=1}^{U} \mathbf{R}_{c,n,u,l} + \sum_{u=1}^{U} \left(\mathbf{R}_{c,n,u,l} - \tilde{\mathbf{R}}_{c,n,u,l}\right) \succeq 0, \tag{56}$$

which implies constraint (24d) holds under (25) and (26).

Finally, let $\mathbf{v} = \mathbf{R}_{c,n,u,l} \mathbf{h}_{n,u,l} \in \mathbb{C}^{M_t \times 1}$ and $\alpha = \mathbf{h}_{n,u,l}^H \mathbf{R}_{c,n,u,l} \mathbf{h}_{n,u,l} \in \mathbb{R}$. Then, we have $\tilde{\mathbf{R}}_{c,n,u,l} = \frac{\mathbf{v}\mathbf{v}^H}{\alpha}$. If $\alpha > 0$, which holds whenever the SINR constraint requires nonzero useful power on user u, subcarrier l for node n, then $\mathbf{v} \neq \mathbf{0}$ and $\mathbf{v}\mathbf{v}^H$ is a nonzero rank-one matrix. Since scaling by a nonzero scalar does not change rank, $\operatorname{rank}(\tilde{\mathbf{R}}_{c,n,u,l}) = 1$, thus completing the proof.

References

[1] K. Han, K. Meng, and C. Masouros, "Transmit Beamforming Design for Noncoherent Distributed Integrated Sensing and Communication Systems," in *Proceedings of the IEEE Radar Conference*. IEEE, 2025.

[2] J. A. Zhang, F. Liu, C. Masouros, R. W. Heath, Z. Feng, L. Zheng, and A. Petropulu, "An Overview of Signal Processing Techniques for Joint Communication and Radar Sensing," *IEEE Journal of Selected Topics in Signal Processing*, vol. 15, no. 6, pp. 1295–1315, 2021.

[3] F. Liu, Y. Cui, C. Masouros, J. Xu, T. X. Han, Y. C. Eldar, and S. Buzzi, "Integrated Sensing and Communications: Toward Dual-Functional Wireless Networks for 6G and Beyond," *IEEE Journal on Selected Areas in Communications*, vol. 40, no. 6, pp. 1728–1767, 2022.

[4] J. A. Zhang, M. L. Rahman, K. Wu, X. Huang, Y. J. Guo, S. Chen, and J. Yuan, "Enabling joint communication and radar sensing in mobile networks—a survey," *IEEE Communications Surveys & Tutorials*, vol. 24, no. 1, pp. 306–345, 2021.

[5] T. Wild, V. Braun, and H. Viswanathan, "Joint Design of Communication and Sensing for Beyond 5G and 6G Systems," *IEEE Access*, vol. 9, pp. 30 845–30 857, 2021.

[6] D. Ma, N. Shlezinger, T. Huang, Y. Liu, and Y. C. Eldar, "Joint Radar-Communication Strategies for Autonomous Vehicles: Combining Two Key Automotive Technologies," *IEEE Signal Processing Magazine*, vol. 37, no. 4, pp. 85–97, 2020.

[7] Z. He, W. Xu, H. Shen, D. W. K. Ng, Y. C. Eldar, and X. You, "Full-duplex communication for ISAC: Joint beamforming and power optimization," *IEEE Journal on Selected Areas in Communications*, vol. 41, no. 9, pp. 2920–2936, 2023.

[8] B. Li and A. P. Petropulu, "Joint transmit designs for coexistence of MIMO wireless communications and sparse sensing radars in clutter," *IEEE Transactions on Aerospace and Electronic Systems*, vol. 53, no. 6, pp. 2846–2864, 2017.

[9] N. T. Nguyen, N. Shlezinger, Y. C. Eldar, and M. Juntti, "Multiuser MIMO wideband joint communications and sensing system with subcarrier allocation," *IEEE Transactions on Signal Processing*, 2023.

[10] F. Liu, L. Zhou, C. Masouros, A. Li, W. Luo, and A. Petropulu, "Toward dual-functional radar-communication systems: Optimal waveform design," *IEEE Transactions on Signal Processing*, vol. 66, no. 16, pp. 4264–4279, 2018.

[11] I. Valiulahi, C. Masouros, and A. Salem, "Net-zero energy dual-functional radar-communication systems," *IEEE Transactions on Green Communications and Networking*, vol. 7, no. 1, pp. 356–369, 2023.

[12] F. Dong, F. Liu, Y. Cui, W. Wang, K. Han, and Z. Wang, "Sensing as a service in 6G perceptive networks: A unified framework for ISAC resource allocation," *IEEE Transactions on Wireless Communications*, vol. 22, no. 5, pp. 3522–3536, 2022.

[13] Z. Wei, H. Liu, Z. Feng, H. Wu, F. Liu, Q. Zhang, and Y. Du, "Deep cooperation in isac system: Resource, node and infrastructure perspectives," *IEEE Internet of Things Magazine*, 2024.

[14] E. C. Strinati, G. C. Alexandropoulos, N. Amani, M. Crozzoli, G. Madhusudan, S. Mekki, F. Rivet, V. Sciancalepore, P. Sehier, M. Stark *et al.*, "Towards Distributed and Intelligent Integrated Sensing and Communications for 6G Networks," *arXiv preprint arXiv:2402.11630*, 2024.

[15] X. Zhu, J. Liu, L. Lu, T. Zhang, T. Qiu, C. Wang, and Y. Liu, "Enabling intelligent connectivity: A survey of secure ISAC in 6G networks," *IEEE Communications Surveys & Tutorials*, 2024.

[16] R. Thomä and T. Dallmann, "Distributed ISAC systems–multisensor radio access and coordination," in *2023 20th European Radar Conference (EuRAD)*. IEEE, 2023, pp. 351–354.

[17] K. Meng, C. Masouros, A. P. Petropulu, and L. Hanzo, "Cooperative ISAC Networks: Opportunities and Challenges," *IEEE Wireless Communications*, pp. 1–8, 2024.

[18] K. Meng, C. Masouros, G. Chen, and F. Liu, "Network-Level Integrated Sensing and Communication: Interference Management and BS Coordination Using Stochastic Geometry," *IEEE Transactions on Wireless Communications*, vol. 23, no. 12, pp. 19 365–19 381, 2024.

[19] K. Meng, K. Han, C. Masouros, and L. Hanzo, "Network-level ISAC: An Analytical Study of Antenna Topologies Ranging from Massive to Cell-Free MIMO," *IEEE Transactions on Wireless Communications*, 2025.

[20] X. Lou, W. Xia, S. Jin, and H. Zhu, "Beamforming Optimization in Distributed ISAC System with Integrated Active and Passive Sensing," *IEEE Transactions on Communications*, 2024.

[21] W. Jiang, Z. Wei, S. Yang, Z. Feng, and P. Zhang, "Cooperation based joint active and passive sensing with asynchronous transceivers for perceptive mobile networks," *IEEE Transactions on Wireless Communications*, 2024.

[22] A. Chowdary, A. Bazzi, and M. Chafii, "On hybrid radar fusion for integrated sensing and communication," *IEEE Transactions on Wireless Communications*, 2024.

[23] Z. Zhang, H. Ren, C. Pan, S. Hong, D. Wang, J. Wang, and X. You, "Target Localization in Cooperative ISAC Systems: A Scheme Based on 5G NR OFDM Signals," *IEEE Transactions on Communications*, 2024.

[24] Z. Wei, H. Liu, H. Li, W. Jiang, Z. Feng, H. Wu, and P. Zhang, "Integrated Sensing and Communication Enabled Cooperative Passive Sensing Using Mobile Communication System," *arXiv preprint arXiv:2405.09179*, 2024.

[25] X. Yang, Z. Wei, J. Xu, Y. Fang, H. Wu, and Z. Feng, "Coordinated Transmit Beamforming for Networked ISAC with Imperfect CSI and Time Synchronization," *IEEE Transactions on Wireless Communications*, 2024.

[26] K. Ji, Q. Zhang, Z. Wei, Z. Feng, and P. Zhang, "Networking based ISAC hardware testbed and performance evaluation," *IEEE Communications Magazine*, vol. 61, no. 5, pp. 76–82, 2023.

[27] B. Wang, Y. Wang, N. Li, J. Zhu, X. She, and P. Chen, "On Collaborative Sensing of Cellular Networks Under Mutual Signal Interference," *IEEE Wireless Communications Letters*, 2024.

[28] P. Gao, L. Lian, and J. Yu, "Cooperative ISAC with direct localization and rate-splitting multiple access communication: A pareto optimization framework," *IEEE Journal on Selected Areas in Communications*, vol. 41, no. 5, pp. 1496–1515, 2023.

[29] D. Xu, C. Liu, S. Song, and D. W. K. Ng, "Integrated sensing and communication in coordinated cellular networks," in *2023 IEEE Statistical Signal Processing Workshop (SSP)*. IEEE, 2023, pp. 90–94.

[30] U. Demirhan and A. Alkhateeb, "Cell-free ISAC MIMO systems: Joint sensing and communication beamforming," *IEEE Transactions on Communications*, 2024.

[31] K. Zhang, Y. Xu, R. He, C. Shen, and T.-h. Chang, "Optimal joint fronthaul compression and beamforming design for networked ISAC systems," *arXiv preprint arXiv:2408.08057*, 2024.

[32] N. Babu, C. Masouros, C. B. Papadias, and Y. C. Eldar, "Precoding for multi-cell ISAC: from coordinated beamforming to coordinated multipoint and bi-static sensing," *arXiv preprint arXiv:2402.18387*, 2024.

[33] H. Godrich, A. M. Haimovich, and R. S. Blum, "Target localization accuracy gain in MIMO radar-based systems," *IEEE Transactions on Information Theory*, vol. 56, no. 6, pp. 2783–2803, 2010.

[34] H. Dahrouj and W. Yu, "Coordinated beamforming for the multicell multi-antenna wireless system," *IEEE transactions on wireless communications*, vol. 9, no. 5, pp. 1748–1759, 2010.

[35] R. Irmer, H. Droste, P. Marsch, M. Grieger, G. Fettweis, S. Brueck, H.-P. Mayer, L. Thiele, and V. Jungnickel, "Coordinated multipoint: Concepts, performance, and field trial results," *IEEE Communications Magazine*, vol. 49, no. 2, pp. 102–111, 2011.

[36] W. Zhu, S. Zhang, and L. Liu, "Joint Transmission and Compression Optimization for Networked Sensing with Limited-Capacity Fronthaul Links," *IEEE Transactions on Wireless Communications*, 2025.

[37] S. Gogineni and A. Nehorai, "Target estimation using sparse modeling for distributed MIMO radar," *IEEE Transactions on Signal Processing*, vol. 59, no. 11, pp. 5315–5325, 2011.

[38] O. Kanhere, S. Goyal, M. Beluri, and T. S. Rappaport, "Target localization using bistatic and multistatic radar with 5G NR waveform," in *2021 IEEE 93rd Vehicular Technology Conference (VTC2021-Spring)*. IEEE, 2021, pp. 1–7.

[39] Y. Yang and R. S. Blum, "Phase synchronization for coherent MIMO radar: Algorithms and their analysis," *IEEE Transactions on Signal Processing*, vol. 59, no. 11, pp. 5538–5557, 2011.

[40] D. Xu, Y. Xu, X. Zhang, X. Yu, S. Song, and R. Schober, "Interference mitigation for network-level ISAC: An optimization perspective," *IEEE Communications Magazine*, vol. 62, no. 9, pp. 28–34, 2024.

[41] B. Hofmann-Wellenhof, H. Lichtenegger, and J. Collins, *Global positioning system: theory and practice*. Springer Science & Business Media, 2012.

[42] K. Alemdar, D. Varshney, S. Mohanti, U. Muncuk, and K. Chowdhury, "RFClock: Timing, phase and frequency synchronization for distributed wireless networks," in *Proceedings of the 27th Annual International Conference on Mobile Computing and Networking*, 2021, pp. 15–27.

[43] K. Han, S. Kang, and S. Hong, "Sub-Nyquist Sampling OFDM Radar," *IEEE Transactions on Radar Systems*, vol. 1, pp. 669–680, 2023.

[44] M. Sadeghi, F. Behnia, R. Amiri, and A. Farina, "Target localization geometry gain in distributed mimo radar," *IEEE Transactions on Signal Processing*, vol. 69, pp. 1642–1652, 2021.

[45] H. Zhao, N. Zhang, and Y. Shen, "Beamspace direct localization for large-scale antenna array systems," *IEEE Transactions on Signal Processing*, vol. 68, pp. 3529–3544, 2020.

[46] R. Tanbourgi, S. Singh, J. G. Andrews, and F. K. Jondral, "A tractable model for noncoherent joint-transmission base station cooperation," *IEEE Transactions on Wireless Communications*, vol. 13, no. 9, pp. 4959–4973, 2014.

[47] F. Liu, Y.-F. Liu, A. Li, C. Masouros, and Y. C. Eldar, "Cramér-Rao bound optimization for joint radar-communication beamforming," *IEEE Transactions on Signal Processing*, vol. 70, pp. 240–253, 2021.

[48] X. Liu, T. Huang, N. Shlezinger, Y. Liu, J. Zhou, and Y. C. Eldar, "Joint transmit beamforming for multiuser MIMO communications and MIMO radar," *IEEE Transactions on Signal Processing*, vol. 68, pp. 3929–3944, 2020.

[49] V. Slyusar, "A family of face products of matrices and its properties," *Cybernetics and systems analysis*, vol. 35, no. 3, pp. 379–384, 1999.

[50] F. Zhang, *The Schur complement and its applications*. Springer Science & Business Media, 2006, vol. 4.

[51] N. J. Higham, "Computing a nearest symmetric positive semidefinite matrix," *Linear algebra and its applications*, vol. 103, pp. 103–118, 1988.

[52] ——, "Analysis of the cholesky decomposition of a semi-definite matrix," 1990.

[53] H. Jiang, T. Kathuria, Y. T. Lee, S. Padmanabhan, and Z. Song, "A faster interior point method for semidefinite programming," in *2020 IEEE 61st annual symposium on foundations of computer science (FOCS)*. IEEE, 2020, pp. 910–918.

[54] K. Han, K. Meng, and C. Masouros, "Over-the-air time-frequency synchronization in distributed ISAC systems," *arXiv preprint arXiv:2503.08920*, 2025.

[55] K. Han, K. Meng, X.-Y. Wang, and C. Masouros, "Network-Level ISAC Design: State-of-the-Art, Challenges, and Opportunities," *IEEE J. Sel. Topics Electro., Antennas Propag.*, 2025.

[56] P. Li, M. Li, R. Liu, Q. Liu, and A. L. Swindlehurst, "MIMO-OFDM ISAC waveform design for range-Doppler sidelobe suppression," *IEEE Transactions on Wireless Communications*, 2024.

[57] H. Bolcskei, "MIMO-OFDM wireless systems: basics, perspectives, and challenges," *IEEE wireless communications*, vol. 13, no. 4, pp. 31–37, 2006.

[58] J. Choi, B. Mondal, and R. W. Heath, "Interpolation based unitary precoding for spatial multiplexing MIMO-OFDM with limited feedback," *IEEE Transactions on Signal Processing*, vol. 54, no. 12, pp. 4730–4740, 2006.

[59] T. Pande, D. J. Love, and J. V. Krogmeier, "Reduced feedback MIMO-OFDM precoding and antenna selection," *IEEE Transactions on Signal Processing*, vol. 55, no. 5, pp. 2284–2293, 2007.

[60] C. Xu and S. Zhang, "MIMO integrated sensing and communication exploiting prior information," *IEEE Journal on Selected Areas in Communications*, vol. 42, no. 9, pp. 2306–2321, 2024.

[61] Y. Liu and W. Yu, "MIMO sensing beamforming design with low-resolution transceive," in *IEEE Int. Conf. Commun. (ICC), Montreal, Canada*. IEEE, 2025.

[62] Y. Liu, K. M. Attiah, and W. Yu, "RIS-assisted joint sensing and communications via fractionally constrained fractional programming," *IEEE Transactions on Wireless Communications*, 2025.

[63] X. Li, Q. Zhu, Y. Chen, C. Assi, and Y. Yuan, "Sensing for Communication: RIS-Assisted ISAC Coordination Gain Enhancement With Imperfect CSI," *IEEE Transactions on Wireless Communications*, 2025.